Cell Stem Cell

Short article

m^{6}A/YTHDF2-mediated mRNA decay targets TGF-β signaling to suppress the quiescence acquisition of early postnatal mouse hippocampal NSCs

Graphical abstract

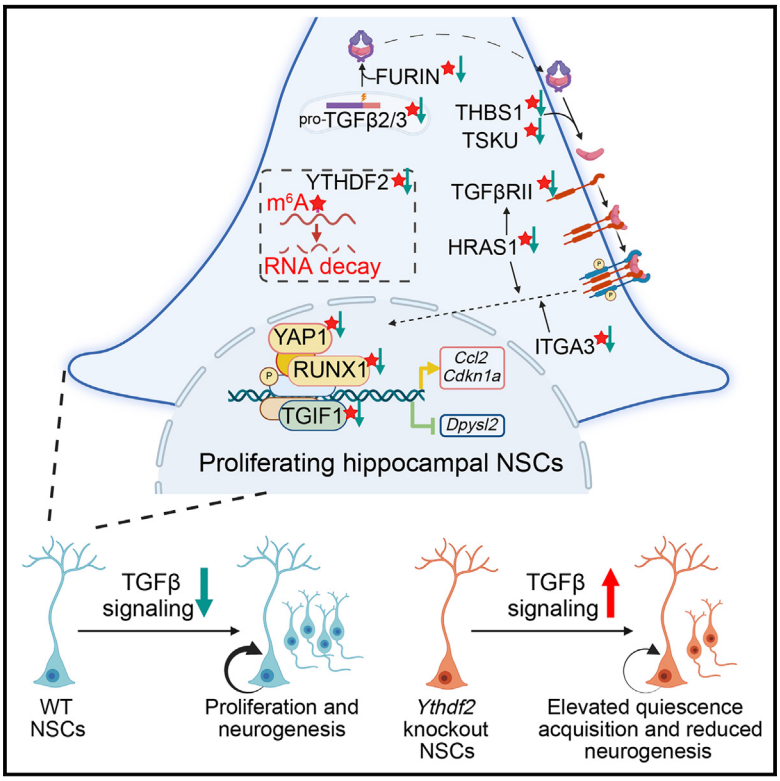

Highlights

- *Ythdf2* deletion elevates quiescence acquisition of hippocampal neural stem cells (NSCs)
- Multiple TGF-β pathway components are m^{6}A, Ythdf2, and mRNA decay targets
- TGF-β-signaling inhibition rescues elevated quiescence acquisition of *Ythdf2* cKO NSCs
- Epitranscriptomic convergent co-regulation of multiple components in a single pathway

Authors

Feng Zhang, Yao Fu, Dennisse Jimenez-Cyrus, ..., Chuan He, Guo-li Ming, Hongjun Song

Correspondence

gming@pennmedicine.upenn.edu (G.-l.M.), shongjun@pennmedicine.upenn.edu (H.S.)

In brief

Zhang et al. revealed a distinct mode of epitranscriptomic control, with convergent co-regulation of multiple components of the same signaling pathway in stem cells. Specifically, m^{6}A/YTHDF2 signaling promotes mRNA decay of multiple TGF-β pathway components, which reduces TGF-β-signaling activation cell autonomously in proliferating neural stem cells to suppress their quiescence acquisition.

Zhang et al., 2025, Cell Stem Cell *32*, 144–156
January 2, 2025
https://doi.org/10.1016/j.stem.2024.10.002

CellPress

CellPress

Cell Stem Cell

Short article

m^{6}A/YTHDF2-mediated mRNA decay targets TGF-β signaling to suppress the quiescence acquisition of early postnatal mouse hippocampal NSCs

Feng Zhang,[1,2] Yao Fu,[3] Dennisse Jimenez-Cyrus,[1] Ting Zhao,[1] Yachen Shen,[1] Yusha Sun,[1] Zhijian Zhang,[1] Qing Wang,[4] Riki Kawaguchi,[4] Daniel H. Geschwind,[4] Chuan He,[5] Guo-li Ming,[1,6,7,8,*] and Hongjun Song[1,6,8,9,10,11,*]

[1]Department of Neuroscience and Mahoney Institute for Neurosciences, Perelman School for Medicine, University of Pennsylvania, Philadelphia, PA, USA
[2]School of Life Sciences, Nanjing University, Nanjing, PRC
[3]Department of Biology, School of Art and Sciences, University of Pennsylvania, Philadelphia, PA, USA
[4]Program in Neurogenetics, Department of Neurology, David Geffen School of Medicine, University of California, Los Angeles, Los Angeles, CA, USA
[5]Department of Chemistry, Department of Biochemistry and Molecular Biology, Howard Hughes Medical Institute, The University of Chicago, Chicago, IL, USA
[6]Department of Cell and Developmental Biology, Perelman School for Medicine, University of Pennsylvania, Philadelphia, PA, USA
[7]Department of Psychiatry, Perelman School for Medicine, University of Pennsylvania, Philadelphia, PA, USA
[8]Institute for Regenerative Medicine, University of Pennsylvania, Philadelphia, PA, USA
[9]The Epigenetics Institute, Perelman School for Medicine, University of Pennsylvania, Philadelphia, PA, USA
[10]Department of Neurosurgery, Perelman School for Medicine, University of Pennsylvania, Philadelphia, PA, USA
[11]Lead contact
*Correspondence: gming@pennmedicine.upenn.edu (G.-l.M.), shongjun@pennmedicine.upenn.edu (H.S.)
https://doi.org/10.1016/j.stem.2024.10.002

SUMMARY

Quiescence acquisition of proliferating neural stem cells (NSCs) is required to establish the adult NSC pool. The underlying molecular mechanisms are not well understood. Here, we showed that conditional deletion of the m^{6}A reader *Ythdf2*, which promotes mRNA decay, in proliferating NSCs in the early postnatal mouse hippocampus elevated quiescence acquisition in a cell-autonomous fashion with decreased neurogenesis. Multimodal profiling of m^{6}A modification, YTHDF2 binding, and mRNA decay in hippocampal NSCs identified shared targets in multiple transforming growth factor β (TGF-β)-signaling-pathway components, including TGF-β ligands, maturation factors, receptors, transcription regulators, and signaling regulators. Functionally, *Ythdf2* deletion led to TGF-β-signaling activation in NSCs, suppression of which rescued elevated quiescence acquisition of proliferating hippocampal NSCs. Our study reveals the dynamic nature and critical roles of mRNA decay in establishing the quiescent adult hippocampal NSC pool and uncovers a distinct mode of epitranscriptomic control via co-regulation of multiple components of the same signaling pathway.

INTRODUCTION

Adult hippocampal neurogenesis contributes to normal brain functions, such as learning, memory, and mood regulation,[1–6] whereas its dysregulation has been associated with various brain disorders.[2,7–10] Quiescent neural stem cells (NSCs) in the adult dentate gyrus (DG) originate from proliferating NSCs, and their quiescence acquisition in the early postnatal mouse DG represents a major milestone in establishing the adult NSC pool.[11–13] Although quiescence of adult NSCs is required to sustain life-long neurogenesis, and mechanisms that regulate adult NSC quiescence maintenance have been extensively investigated,[14] molecular mechanisms regulating quiescence acquisition of proliferating NSCs during early postnatal stages in the DG are not well understood.[15–17]

Both transforming growth factors β (TGF-βs) and bone morphogenetic proteins (BMPs) belong to the TGF-β superfamily.[18] BMP signaling promotes the quiescent state of adult NSCs in the DG *in vivo* and BMP4 treatment switches proliferating adult NSCs to the quiescent state *in vitro*.[15,19] TGF-β signaling also suppresses adult neurogenesis[20,21] and has been implicated in embryonic neurogenesis.[22] For example, TGF-β regulates the temporal identity of NSCs and their differentiation potency toward early- and late-born neurons in the hindbrain.[23] However, the role of the TGF-β superfamily in quiescence acquisition of early postnatal NSCs in the DG is unknown.

Studies of over 170 types of RNA chemical modifications, or epitranscriptomics, have attracted tremendous basic and clinical research interest because of their critical roles in regulating almost every aspect of RNA metabolism (e.g., decay, splicing,

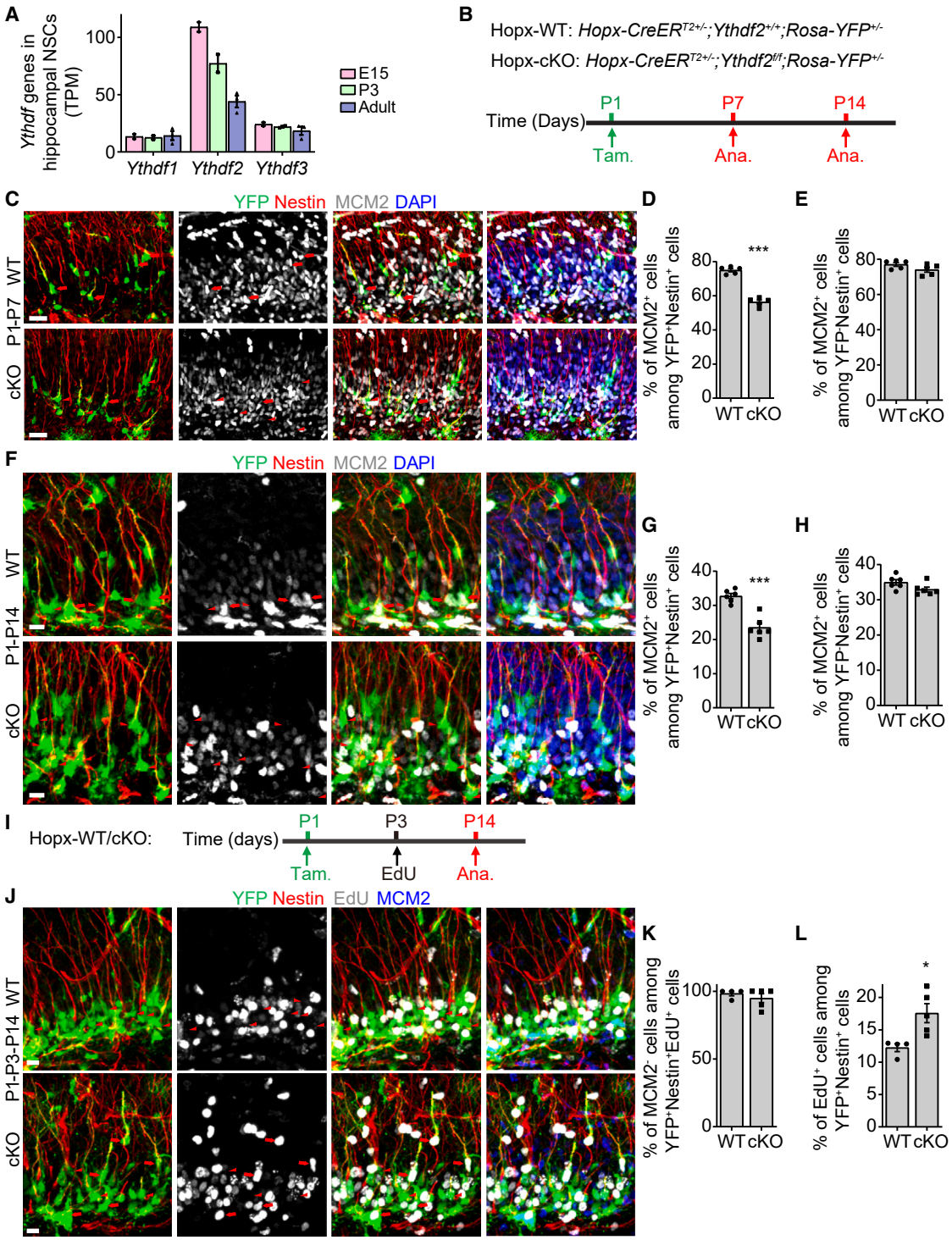

Figure 1. Conditional *Ythdf2* deletion, specifically in early postnatal DG NSCs, promotes their quiescence acquisition

(A) Transcripts per million (TPM) values of *Ythdf*/*Ythdf2*/*Ythdf3* mRNA in FACS-purified NSCs from Hopx-GFP transgenic mouse DG from our published dataset.[11] Values represent mean ± SEM (n = 2/E15; 2/P3; 3/adult).

(B) A schematic diagram of the experimental design.

(C–H) Sample confocal images of staining in the upper blade of DG at P7 (C; scale bars: 20 μm) and P14 (F; scale bars: 10 μm), and quantifications. Red arrows indicate MCM2$^+$YFP$^+$Nestin$^+$ NSCs and red arrowheads indicate MCM2$^-$YFP$^+$Nestin$^+$ NSCs (C and F). Individual dots represent data from each animal (D, E, G, and H). Values represent mean ± SEM (n = 5/P7; 6/P14; ***$p < 0.001$; Student's t test).

(I) A schematic diagram of the EdU-retaining assay.

(legend continued on next page)

stability, transport, alternative polyadenylation, and translation) in diverse biological processes, including in the nervous system,[24–26] as well as their therapeutic potential, such as the success of the COVID-19 mRNA vaccine.[27–29] m^{6}A modification is the most abundant internal chemical modification within eukaryotic mRNAs,[27] and studies have identified its catalytic writers, decoding readers, and erasers.[30,31] One of its key functions is to promote mRNA decay, mainly involving the YTHDF family proteins of m^{6}A reader proteins.[27,32,33] YTHDF family proteins (YTHDF1–3) play important roles in regulating brain development and functions, such as cortical neurogenesis[24] and hippocampus-dependent learning and memory.[34,35] However, roles and mechanisms of m^{6}A- and YTHDF-mediated mRNA decay in regulating the quiescence acquisition of NSCs in the early postnatal DG remain unknown.

Although m^{6}A modification occurs on a large number of mRNAs,[25,36] many previous functional studies suggested that one basic mode of m^{6}A epitranscriptomic regulation of cellular processes is via controlling one or a few key genes.[35,37,38] Here, we used a genetic mouse model to investigate the role and mechanism of YTHDF2 in regulating quiescence acquisition of proliferating NSCs in the early postnatal DG. Our study uncovered a distinct mode of epitranscriptomic control via convergent co-regulation of mRNA decay of multiple components of the TGF-β-signaling pathway as a "gatekeeper" for quiescence acquisition of proliferating NSCs.

RESULTS

Ythdf2 deletion in proliferating DG NSCs leads to elevated quiescence acquisition

We analyzed our published bulk RNA sequencing (RNA-seq) dataset[11] for expression of different m^{6}A readers in DG NSCs at different stages (Figure S1A). Among three YTHDF family genes, *Ythdf2* exhibits the highest expression level at different stages and its expression level gradually decreases from the embryonic to adult stages (Figure 1A). Further analysis of our published single-cell RNA-seq datasets[16,39] revealed a gradual decrease of *Ythdf2* expression along pseudotime of the transition of proliferating NSCs to quiescence from postnatal day 3 (P3) to P14 and, conversely, a gradual increase of *Ythdf2* expression along pseudotime of quiescent NSC activation in the adult DG (Figure S1B). These observations raise the possibility that YTHDF2 may regulate DG NSC quiescence acquisition during the early postnatal stage.

To assess the potential role of YTHDF2, we first confirmed effective deletion of *Ythdf2* in proliferating NSCs at the protein level in our genetic model using cultured NSCs derived from the P0.5 hippocampus and E17.5 embryonic cortex of *Nestin-Cre*$^{+/-}$::*Ythdf2*$^{f/f}$ mice (Nestin-conditional-knockout [cKO] mice) in comparison with those from *Ythdf2*$^{f/f}$ mice[37] (Nestin-wild-type [WT] mice) (Figures S1C–S1E). We then crossed *Ythdf2*$^{f/f}$ mice with *Hopx-CreER*$^{T2+/-}$ mice, which target DG NSCs,[11,17] and *Rosa26*$^{flox\text{-}stop\text{-}flox\text{-}EYFP}$ reporter mice to generate *Hopx-CreER*$^{T2+/-}$::*Ythdf2*$^{f/f}$::*Rosa-YFP*$^{+/-}$ mice (Hopx-cKO mice) and *Hopx-CreER*$^{T2+/-}$::*Ythdf2*$^{+/+}$::*Rosa-YFP*$^{+/-}$ mice (Hopx-WT mice, as controls). Tamoxifen injection at P1 and analysis at P7 and P14 showed that the percentage of MCM2$^+$ cells among the YFP$^+$Nestin$^+$ NSCs, but not among the YFP$^-$Nestin$^+$ NSCs, in the DG was reduced in the Hopx-cKO mice compared with Hopx-WT mice (Figures 1B–1H). MCM2 is a marker of proliferating cells and MCM2$^-$ can be used as an indicator of quiescence.[17,40] Therefore, these results suggest that knockout of *Ythdf2* in proliferating NSCs promotes their quiescence acquisition in a cell-autonomous fashion in the early postnatal DG.

To further support this notion, we performed 5-Ethynyl-2′-deoxyuridine (EdU)-retaining experiments[17] (Figure 1I; see STAR Methods). The percentage of EdU$^+$ cells among YFP$^+$Nestin$^+$ NSCs was similar between Hopx-WT and Hox-cKO mice after 2-h labeling, indicating similar timing of quiescence acquisition and proliferating NSC labeling efficacy by EdU at P3 (Figures S1F and S1G). At P14, nearly all the EdU$^+$YFP$^+$Nestin$^+$ NSCs in both Hopx-cKO and Hopx-WT DG at P14 were MCM2$^-$, confirming the quiescence acquisition of EdU$^+$ NSCs before P14 (Figures 1J and 1K). Importantly, the percentage of YFP$^+$Nestin$^+$ NSCs retaining EdU was higher in Hopx-cKO mice compared with Hopx-WT mice in the DG (Figures 1J and 1L), indicating that the knockout of *Ythdf2* promotes quiescence acquisition of DG NSCs at the early postnatal stage.

We next examined the consequence of elevated quiescence acquisition of NSCs in Hopx-cKO mice. We found decreased percentages of PROX1$^+$ dentate granule neurons among all the YFP$^+$ progeny in Hopx-cKO DG at P7 and P14 compared with Hopx-WT DG (Figures S1H–S1K). All GFP$^+$NeuN$^+$ neurons were PROX1$^+$ in both Hopx-WT and Hopx-cKO mice at P14, indicating no change in the neuronal subtype fate specification (Figures S1L and S1M). Further analysis of Nestin-cKO mice at P30 showed a modest increase in NSC density without an effect on NSC proliferation at P30 compared with Nestin-WT mice (Figures S1N–S1P).

Together, these results indicate that knockout of *Ythdf2* in proliferating DG NSCs during early postnatal stages leads to elevated quiescence acquisition at the expense of reduced dentate granule neuron generation, which, in turn, reduces NSC depletion and results in a modest increase in the adult NSC pool in the DG.

Multimodal analysis reveals YTHDF2-mediated convergent epitranscriptomic co-regulation of mRNA decay of multiple TGF-β-signaling components in hippocampal NSCs

To investigate the underlying YTHDF2-dependent molecular mechanism involving m^{6}A and mRNA decay, we turned to relatively homogeneous cultured Nestin-WT and Nestin-cKO hippocampal NSCs for in-depth sequencing analyses. Consistent with *in vivo* findings, knockout of *Ythdf2* also led to reduced proliferation of hippocampal NSCs *in vitro* (Figures 2A and 2B), which was partially rescued with the expression of WT *Ythdf2*

(J–L) Sample immunostaining confocal images of EdU$^-$YFP$^+$Nestin$^+$MCM2$^-$ NSCs (indicated by red arrowheads) in Hopx-WT DG and EdU$^+$YFP$^+$Nestin$^+$MCM2$^-$ NSCs (indicated by red arrows) in Hopx-cKO DG at P14 (J; scale bars: 10 μm) and quantifications (K and L). Values represent mean ± SEM (n = 4/WT; 5/cKO; *$p < 0.05$; Student's t test).
See also Figure S1.

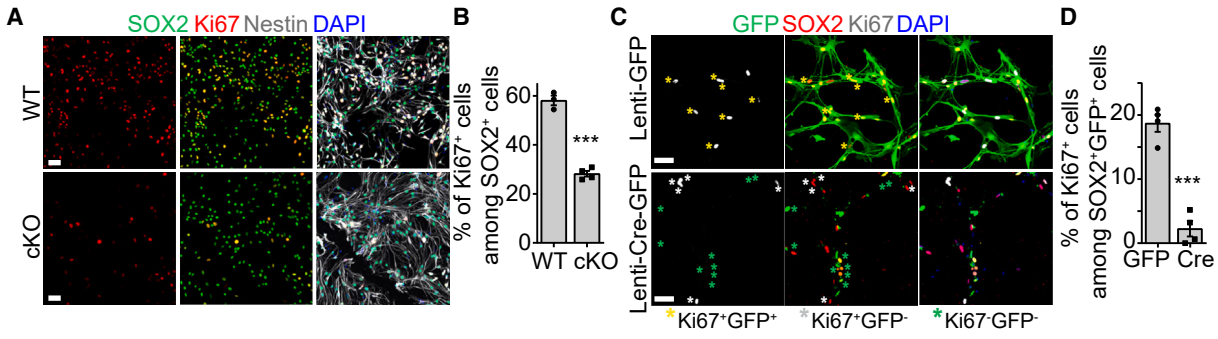

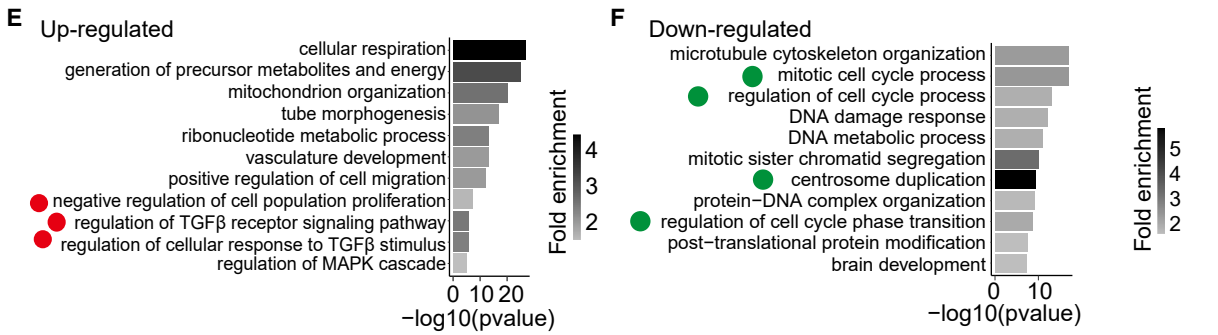

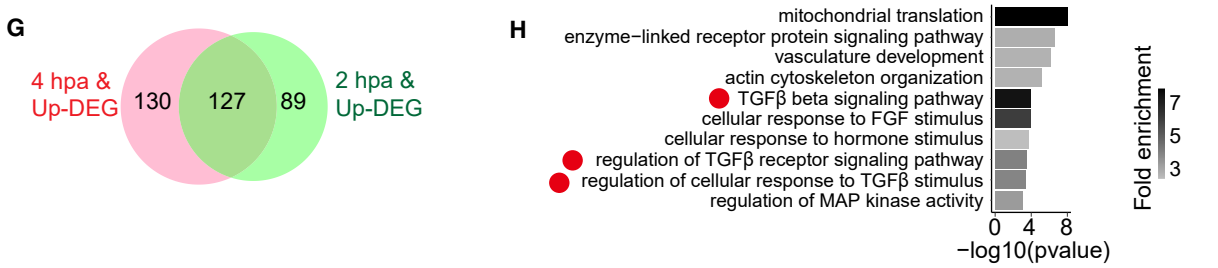

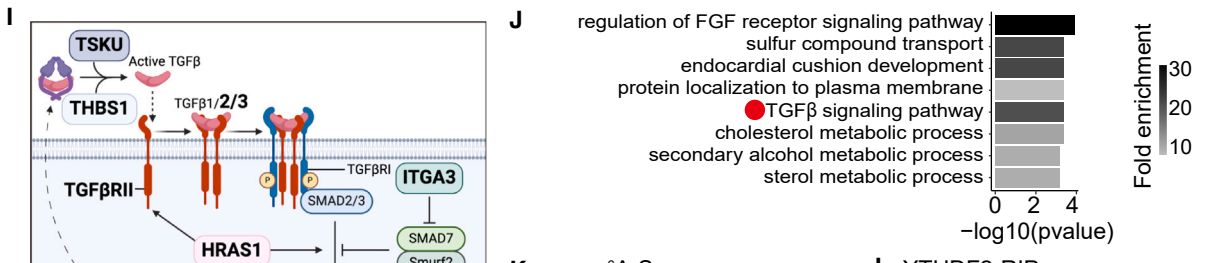

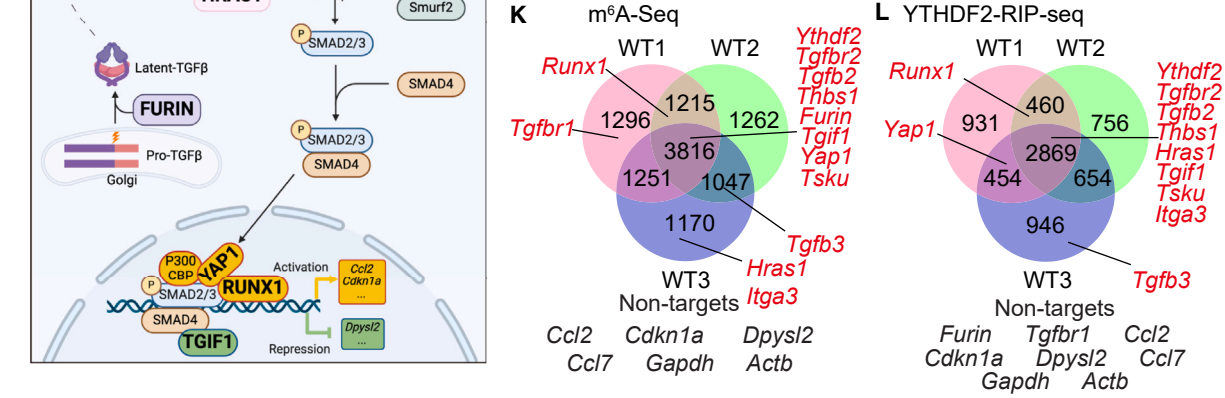

(legend on next page)

(Figures S2A–S2C). Ebselen, an inhibitor that blocks the interaction between YTHDFs and m^{6}A,[41] also decreased proliferation of WT NSCs, with a modest increase in apoptosis (Figures S2D–S2F). To ensure that the effect of YTHDF2 on NSC proliferation was due to m^{6}A-dependent regulation, we deleted m^{6}A methyltransferase *Mettl14*[42] in hippocampal NSCs derived from *Mettl14*$^{f/f}$ mice[25] at P0.5. Compared with expression of GFP alone, lentivirus-mediated expression of Cre-GFP led to a reduced percentage of Ki67$^+$ cells among GFP$^+$SOX2$^+$ NSCs (Figures 2C and 2D), similar to *Ythdf2* cKO NSCs. Together, these results established cultured hippocampal NSCs as a model to examine molecular mechanisms regulating NSC proliferation by m^{6}A and YTHDF2 signaling.

Next, we performed RNA-seq of cultured hippocampal NSCs derived from Nestin-WT and Nestin-cKO mice (Figures S2G and S2H). *Ythdf2* was one of the top upregulated differentially expressed genes (DEGs), indicating that deletion of exon 4 does not induce nonsense-mediated-decay of *Ythdf2* mRNA but triggers a compensatory mechanism to increase the level of remnant *Ythdf2* mRNA (Figure S2H). Gene Ontology (GO) analysis revealed enrichment of the "negative regulation of cell proliferation" term for upregulated DEGs and several cell-cycle-related terms for downregulated DEGs, partially explaining the reduced proliferation of cKO NSCs (Figures 2E and 2F). Notably, several terms related to the TGF-β-signaling pathway were enriched for upregulated DEGs (Figure 2E).

We specifically measured the differential mRNA decay in WT and cKO NSCs with Decay-seq[25] by performing RNA-seq at baseline and 2 and 4 h post actinomycin D treatment (hpa) to inhibit *de novo* transcription (Figure S2I). We identified 346 genes that exhibited both slower decay at either 2 or 4 hpa and upregulated expression at baseline (0 hpa) in cKO NSCs compared with WT NSCs (Figure 2G), GO analysis of which also showed several terms related to TGF-β signaling (Figure 2H).

Canonical TGF-β-signaling activation involves binding of TGF-β ligands to TGF-β receptors II (TGFBR2), which induces the transphosphorylation of the TGFBR1 receptor and consequent phosphorylation of downstream SMAD2/3 proteins, which is inhibited by SMAD7[18,43–47] (Figure 2I). Phosphorylated SMAD2/3 then forms a complex with SMAD4, translocates to the nucleus and binds to diverse transcription activators or repressors, leading to activation (e.g., *Ccl2* and *Cdkn2a*) or repression (e.g., *Dpysl2*) of TGF-β-signaling target genes[18,43–47] (Figure 2I). Multiple components at different steps of the TGF-β-signaling activation pathway were among these baseline-upregulated slower-decay genes in cKO NSCs, including TGF-β ligands (*Tgfb2* and *Tgfb3*); TGF-β maturation and activation factors (*Furin*, a protease in the Golgi apparatus mediating the proteolytic cleavage of the TGF-β precursor polypeptide for its activation[48]; and *Thbs1*, which releases the mature TGF-β from the latent complex[49]); the TGF-β receptor (*Tgfbr2*); SMAD-binding transcription regulators (*Runx1*, a transcription factor and binding partner of SMAD2/3, which promotes TGF-β/SMAD2/3-signaling activation[50,51]; *Yap1*, which binds to SMAD2/3 and mediates their nuclear translocation, thus regulating TGF-β-SMAD signaling[52,53]; and *Tgif1*, a transcriptional corepressor that mediates TGF-β-signaling activation and induces the repression of some TGF-β target genes[47,54,55]); and TGF-β-signaling modulators (*Hras1*, a small GTPase of rat sarcoma virus [RAS] subfamily that enhances TGF-β signaling by stabilizing TGFBR2[56]; *Itga3*, an integrin that enhances TGF-β-signaling activation by repressing SMAD7[57]; and *Tsku*, which positively regulates TGF-β-signaling activation by directly interacting with the TGF-β1 ligand and modulating its activity[58]) (Figures 2I, S2H, S2J, and S2K). We collectively named these identified YTHDF2-regulated multiple TGF-β-signaling components as YMTCs.

To examine whether these YMTCs are direct targets of m^{6}A modification and YTHDF2, we performed m^{6}A-seq and YTHDF2-RNA-Immunoprecipitation-Sequencing (YTHDF2-RIP-seq) of cultured WT hippocampal NSCs (Figures S2L and S2M). There was substantial overlap between YTHDF2-bound and m^{6}A-tagged transcripts (Figure S2N) and between these transcripts and those showing significantly upregulated expression and slower decay in cKO compared with WT NSCs (Figure S2O). Across the transcriptome, the YTHDF2-bound and/or m^{6}A-tagged transcripts, but not the rest of the transcriptome, exhibited significantly slower decay in cKO compared with WT NSCs (Figure S2P). TGF-β-signaling-related terms were

Figure 2. Multimodal sequencing analyses identify multiple components of the TGF-β-signaling pathway as targets regulated by m^{6}A- and YTHDF2-mediated mRNA decay in cultured hippocampal NSCs

(A and B) Sample confocal images of staining in cultured hippocampal NSCs derived from Nestin-WT and Nestin-cKO mice at P0.5 (A; scale bars: 50 μm) and quantifications (B). Dots represent data from each animal (B). Values represent mean ± SEM (n = 3/WT; 4/cKO; $^{**}p < 0.01$; Student's t test).

(C and D) Sample confocal images of immunostaining in hippocampal NSCs derived from *Mettl14*$^{f/f}$ mice at P0.5, infected with GFP- or Cre-GFP-expressing lentivirus and examined 5 days later (C; scale bars: 50 μm), and quantifications (D). Stars represent different types of cells (C). Values represent mean ± SEM (n = 4; $^{***}p < 0.001$; Student's t test).

(E and F) Bar plots of the selective enriched Gene Ontology (GO) terms for biological process of significantly upregulated (E, $p$adj < 0.1, fold-change > 1.5) and downregulated (F, $p$adj < 0.1, fold-change < 2/3) genes in Nestin-cKO compared with Nestin-WT NPCs at 0 hpa. Red (E) and green (F) circles highlight the GO terms of interest.

(G) Venn diagrams showing significantly upregulated genes at 0 hpa and slower-decay genes at 2 or 4 hpa in Nestin-cKO NSCs compared with Nestin-WT NSCs.

(H) Bar plots of the selective enriched GO terms for biological process and pathway terms of 346 genes that exhibited significantly slower decay and significant upregulation in Nestin-cKO compared with Nestin-WT NSCs.

(I) A schematic diagram showing the TGF-β-signaling pathway. Genes shown in bold font indicate multiple TGF-β-signaling components, which exhibited significantly slower decay and upregulation in Nestin-cKO compared with Nestin-WT NSCs.

(J) Bar plots of the selective enriched GO terms for biological process and pathway terms of the overlapping genes between YTHDF2-bound genes, m^{6}A-tagged genes, and significantly upregulated genes with slower decay in cKO NSCs compared with WT NSCs.

(K and L) Venn diagrams showing the overlap of m^{6}A-tagged transcripts (K) or YTHDF2-bound (L) transcripts, identified from m^{6}A-seq or YTHDF2-RIP-seq data of three biological replicates, respectively. Red color indicates m^{6}A-IP or YTHDF2-IP target genes and black color indicates m^{6}A-IP or YTHDF2-IP non-target genes, including housekeeping genes and TGF-β-signaling target genes.

See also Figure S2 and Table S2.

enriched in the GO analysis of the overlapping transcripts that were YTHDF2 bound, m^{6}A tagged, and upregulated with slower decay in cKO NSCs (Figures 2J and S2O). All identified YMTCs harbored m^{6}A modification (Figure 2K) and the majority were bound by YTHDF2 (Figure 2L) in at least one replicate. In contrast, neither the TGF-β-signaling target genes (e.g., *Ccl2*, *Cdkn2a*, and *Dpysl2*) nor housekeeping genes (e.g., *Gapdh* and *Actb*) were among the m^{6}A-tagged and YTHDF2-bound transcripts in NSCs (Figures 2K and 2L). Notably, *Ythdf2* is also m^{6}A modified and YTHDF2 bound (Figures 2K and 2L) and exhibited a baseline upregulation and slower decay in cKO NSCs (Figures S2J and S2K).

To verify our multimodal sequencing results, we performed targeted qPCR validation using independent samples. We confirmed that nearly all identified YMTCs were upregulated in cKO compared with WT NSCs, except for a trend of upregulation of *Tgfb2/3* (Figure 3A). The majority of these YMTCs were also both m^{6}A modified and YTHDF2 bound (Figures 3B and 3C) and exhibited slower decay in cKO compared with WT NSCs at 2 or 4 hpa (Figure 3D). Integrative Genomics Viewer (IGV) views and relative expression levels of several YMTC genes (including *Tgfbr2*), and *Ythdf2* (Figures 3E, 3F, and S3A–S3D) exemplify our multimodal sequencing results. We further validated the elevated expression of TGFBR2 at the protein level in Nestin-cKO NSCs (Figures 3G and 3H).

Although some YMTCs, such as *Tgfb2*, exhibited relatively modest baseline upregulation and slower decay in the cKO NSCs (Figures 3A and 3D), the combined effects from the change of multiple components of TGF-β-signaling pathway could lead to robust activation of TGF-β signaling. Indeed, we found an elevated ratio of phosphorylated (p-)SMAD2 versus total SMAD2 in cKO compared with WT NSCs, indicating TGF-β-signaling activation (Figures 3G and 3H). Moreover, there were corresponding changes in the expression of several TGF-β target genes in cKO NSCs (Figure S3E), which were not m^{6}A-modified, YTHDF2-bound, or slower-decay transcripts in cKO NSCs (Figures 2I, 2K, 2L, S2J, and S2K), excluding the possibility that their expression changes in cKO NSCs were due to m^{6}A-mediated mRNA decay. In addition, overexpression of *Ythdf2* could partially restore the elevated ratio of p-SMAD2/SMAD2 in cKO NSCs (Figures S3F and S3G), whereas treatment of Ebselen in WT NSCs or *Mettl14* cKO NSCs exhibited an elevated ratio of p-SMAD2/SMAD2 (Figures S3H–S3M).

Together, these results revealed that m^{6}A modification and YTHDF2-mediated mRNA decay regulate multiple components of the TGF-β-signaling axis. Although many components are modulated only to a minor degree, all together the multiple points of impact can lead to robust regulation of the TGF-β-signaling pathway in hippocampal NSCs.

Inhibition of TGF-β signaling suppresses *Ythdf2*-deletion-induced elevation of quiescence acquisition in proliferating hippocampal NSCs

To investigate whether *Ythdf2* deletion promotes quiescence acquisition through upregulating TGF-β signaling in hippocampal NSCs, we asked whether activation of TGF-β signaling is sufficient to regulate their proliferation. Treatment with TGF-β2 (100 ng/mL) upregulated the ratio of p-SMAD2/SMAD2 and led to reduced proliferation of WT NSCs, similar to *Ythdf2* cKO NSCs, but did not further affect the proliferation of *Ythdf2* cKO NSCs (Figures 4A–4C and S4A–S4D). Furthermore, treatment with TGF-β-signaling-inhibitor SB-431542 reversed the upregulated TGF-β signaling in *Ythdf2* cKO NSCs (Figures S4E–S4H) and partially rescued their reduced proliferation without affecting apoptosis (Figures 4A–4C).

Next, we investigated the *in vivo* role of TGF-β signaling in the early postnatal DG. Daily intraperitoneal injections of SB-431542[59–61] from P4 to P7 led to a decreased ratio of p-SMAD2/SMAD2 in the hippocampus (Figures 4D, S4I, and S4J) and rescued the decreased percentage of MCM2$^+$ cells among YFP$^+$Nestin$^+$ NSCs in Hopx-cKO mice to similar levels as in Hopx-WT mice at P7 (Figures 4E and 4F). Furthermore, long-term TGF-β-signaling inhibition with SB-431542 injections from P4 to P14 in WT mice increased the percentage of MCM2$^+$ cells among HOPX$^+$Nestin$^+$ NSCs at P14 (Figures 4G–4I, S4K, and S4L), indicating an important role of endogenous TGF-β signaling in the quiescence acquisition of hippocampal NSCs at later stages from P7 to P14.

Together, consistent results from *in vitro* and *in vivo* analyses suggest that knockout of *Ythdf2* promotes quiescence acquisition of early postnatal hippocampal NSCs, at least partially, through enhancing activation of the TGF-β-signaling pathway.

DISCUSSION

Our study reveals that convergent epitranscriptomic inhibition of the TGF-β-signaling pathway in proliferating NSCs suppresses their quiescence acquisition during early postnatal stages in the mouse DG. m^{6}A modification of multiple components of the TGF-β-signaling axis, including TGF-β ligands, receptors, maturation factors, transcription regulators, and signaling regulators, can be recognized by YTHDF2, leading to enhanced mRNA decay and resulting in suppression of TGF-β signaling in proliferating NSCs. Our study identifies a molecular mechanism that suppresses quiescence acquisition of proliferating NSCs in the early postnatal DG, and, together with previous findings,[15–17] it suggests that the process and level of quiescence acquisition of proliferating NSCs is not fixed but instead dynamically controlled by both positive and negative regulators, with functional consequences on the level of developmental neurogenesis and size of the adult NSC pool. We further reveal a distinct molecular logic of epitranscriptomic co-regulation of multiple components of a single signaling pathway.

Quiescence is one major hallmark of adult NSCs in the mammalian brain.[14] Little is known about the molecular mechanism regulating quiescence acquisition of proliferating NSCs to establish the adult NSC pool, which is the foundation for continuous adult neurogenesis throughout life. Previous studies with conditional deletion of *Nkcc1*,[17] a chloride importer that regulates GABA responses,[62] and *Atg7*[15] or *Atg5*,[16] critical components of the autophagy pathway,[63] showed reduced quiescence acquisition of proliferating NSCs during the early postnatal stages, which was interpreted as evidence that these pathways are required for quiescence acquisition. In contrast, we identified YTHDF2-dependent TGF-β-signaling suppression in proliferating NSCs that attenuates their quiescence acquisition, indicating a negative regulator and gatekeeper. Based on our findings, the previous results can be interpreted as NKCC1 and

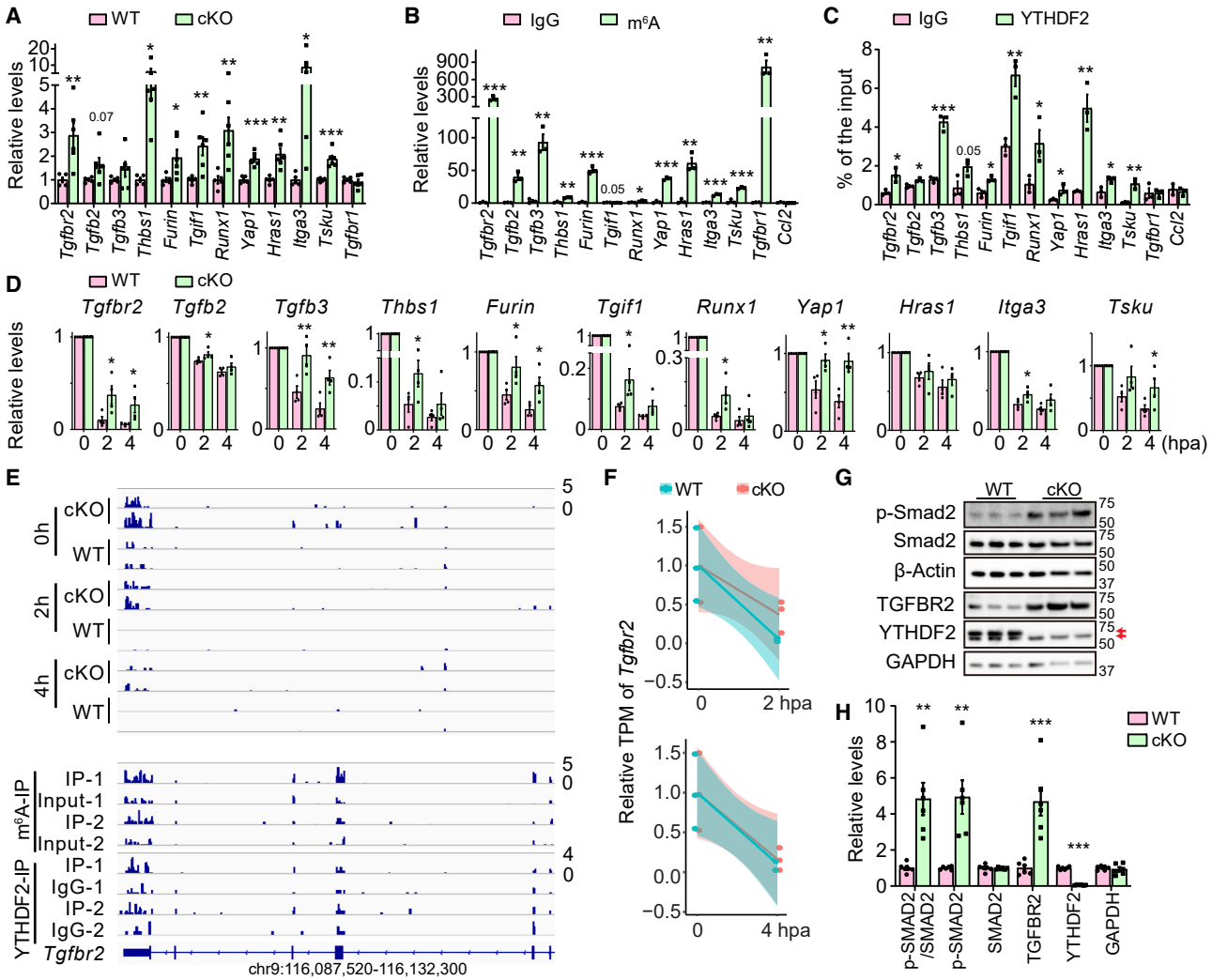

Figure 3. Validation of m^{6}A and YTHDF2 targets in the TGF-β-signaling pathway and slower decay and activation of the TGF-β-signaling pathway in Nestin-cKO NSCs *in vitro*

(A) qPCR analysis of expression levels of YMTCs and *Ythdf2* in Nestin-WT and Nestin-cKO NSCs. *Gapdh* was used as the internal control for normalization. Values represent mean ± SEM (n = 5/WT; 6/cKO; *p < 0.05; **p < 0.01; ***p < 0.001; Student's t test).

(B) qPCR analysis of the levels of YMTCs and *Ythdf2* in the IgG- and m^{6}A-pull-down samples of the cultured Nestin-WT NSCs. For m^{6}A-IP, 10 ng *in vitro*-transcribed *GFP* mRNA was added to 2.5 μg RNA. Enrichment fold of all genes in m^{6}A-pull-down compared with IgG samples was normalized by that of *GFP*. Values represent mean ± SEM (n = 3; *p < 0.05; **p < 0.01; ***p < 0.001; Student's t test).

(C) qPCR analysis of the levels of YMTCs and *Ythdf2* in the IgG- and YTHDF2-pull-down samples of the cultured Nestin-WT NSCs. For YTHDF2-IP, 17.5 ng *in vitro*-transcribed *GFP* mRNA was added for each experiment. The levels of genes were first normalized to input, and enrichment fold of all genes in YTHDF2-pull-down compared with IgG samples was normalized by that of *GFP*. Values represent mean ± SEM (n = 3; *p < 0.05; **p < 0.01; ***p < 0.001; Student's t test).

(D) qPCR analysis of expression levels of YMTC genes in NSCs at 0, 2, and 4 hpa, after being normalized to that at 0 hpa. *Gapdh* was used as the internal control. Values represent mean ± SEM (n = 4; *p < 0.05; **p < 0.01; one-tail Student's t test).

(E) IGV views of *Tgfbr2* in RNA-seq, m^{6}A-seq, and YTHDF2-RIP-seq as an example.

(F) Dot plots of TPM of *Tgfbr2* in Nestin-WT and Nestin-cKO NSCs at 2 and 4 hpa, after being normalized to that at 0 hpa. Linear regression was used to indicate the change between WT and cKO groups.

(G and H) Upregulated TGF-β signaling in the cultured Nestin-cKO NSCs compared with Nestin-WT NSCs. Shown are sample western blot images (G) and quantifications (H). Note the unspecific lower band indicated by the lower red arrow (G), similar to Figure S1D. The intensity was normalized to that of β-actin and then compared with WT samples. Values represent mean ± SEM (n = 6; **p < 0.01; ***p < 0.001; Student's t test).

See also Figures S1 and S3 and Table S1.

ATG5/7 being positive regulators of quiescence acquisition and, together, these results suggest a concept that the process and level of quiescence acquisition of proliferating NSCs during early postnatal stages in the DG is not hard-wired but instead dynamically regulated and balanced by both positive and negative regulators, with functional consequences. Our current study showed that elevated NSC quiescence acquisition from *Ythdf2* cKO leads to decreased generation of dentate granule neurons

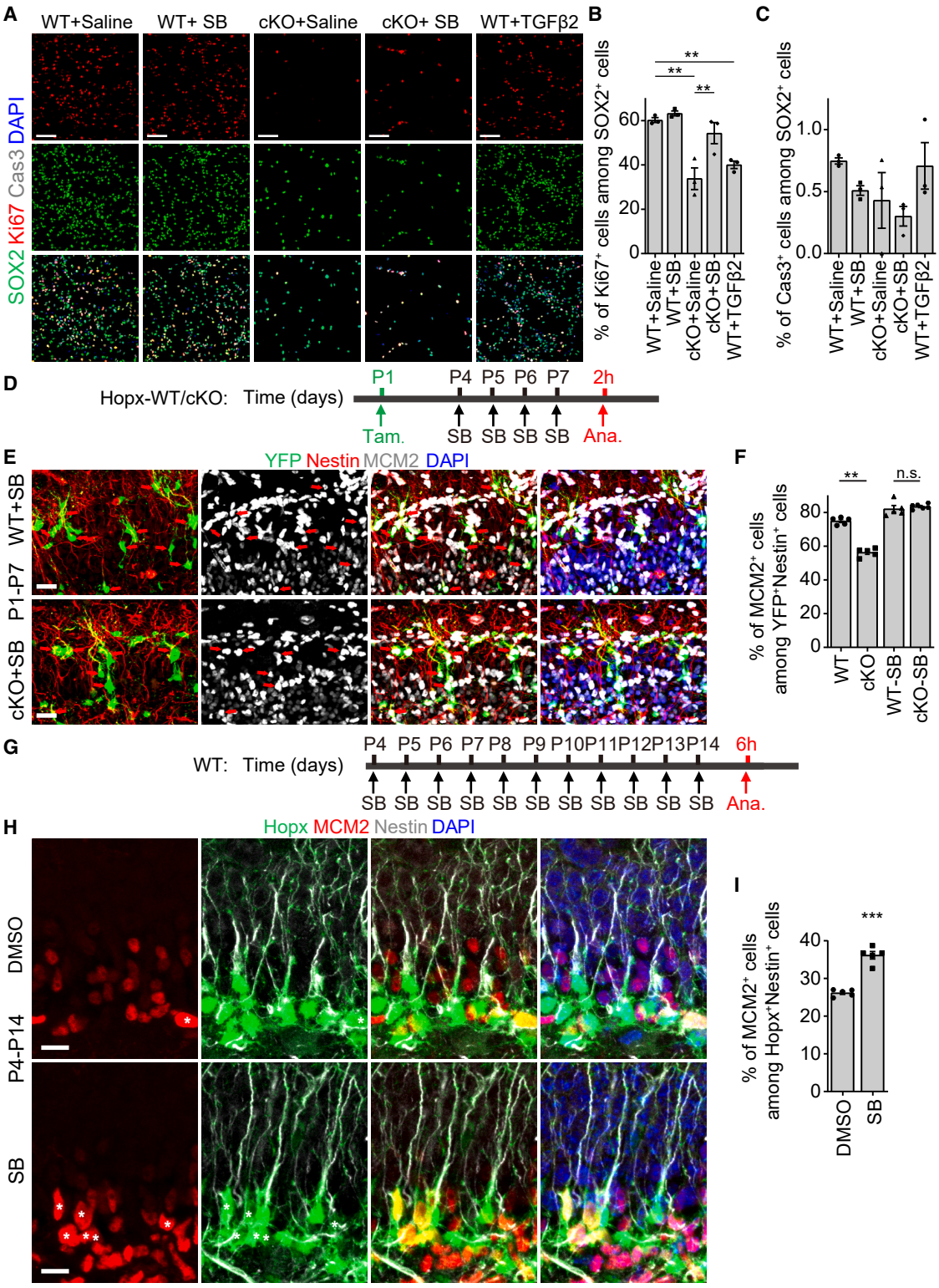

Figure 4. Pharmacological inhibition of TGF-β signaling partially rescues the decreased proliferation *in vitro* and elevated quiescence acquisition *in vivo* for hippocampal NSCs with conditional *Ythdf2* deletion

(A–C) Sample confocal images of immunostaining in cultured Nestin-WT and Nestin-cKO NSCs with treatment of saline (sal), SB-431542 (SB; 5 μM), or TGF-β2 (100 ng/mL) for 48 h (A; scale bar: 50 μm), and quantifications (B and C). Values represent mean ± SEM (n = 3; ns: $p > 0.05$; $^{**}p < 0.01$; $^{***}p < 0.001$; one-way ANOVA).

(legend continued on next page)

and a modest increase in the adult NSC pool. Conversely, decreased NSC quiescence acquisition from *Nkcc1* cKO or *Atg7* or *Atg5 cKO* leads to increased generation of dentate granule neurons and a decreased adult NSC pool.[15–17] It will be interesting in the future to investigate how such processes may be regulated by external stimuli or genetic risk factors for various brain disorders.

Here, we showed that TGF-β ligand treatment suppresses the proliferation of cultured early postnatal hippocampal NSCs *in vitro* and treatment with the TGF-β-signaling inhibitor, SB-431542, partially rescued the reduced proliferation *in vitro* and elevated quiescence acquisition of *Ythdf2* cKO NSCs *in vivo*, indicating that YTHDF2 suppresses quiescence acquisition of NSCs, at least partially, through inhibiting TGF-β signaling. We favor the model that YTHDF2-dependent TGF-β-signaling suppression reduces the amount of quiescence acquisition, instead of just the timing, given the minor difference in quiescence acquisition at P3 (Figures S1F and S1G) and a modest increase of the quiescent NSC pool at P30 (Figures S1N and S1O) upon *Ythdf2* deletion. The essential role of endogenous TGF-β signaling in quiescence acquisition, especially at later stages from P7 to P14, was further demonstrated by effects from the long-term treatment of a TGF-β-signaling inhibitor (Figures 4G–4I). Both TGF-β and BMP signaling have been shown to regulate adult NSC quiescence.[15,19–21] In contrast to many components of the TGF-β-signaling pathway, the majority of BMP pathway components are not m^{6}A tagged or YTHDF2 bound in WT NSCs, and they do not exhibit elevated expression or slower decay in *Ythdf2* cKO compared with WT NSCs (Figure S2O; Table S2). Thus, the BMP pathway is not subject to the same epitranscriptomic m^{6}A/YTHDF2 co-regulation as the TGF-β pathway during the quiescence acquisition of NSCs in the early postnatal DG. Although BMP signaling in adulthood likely originates from the adult neurogenic niche, our current study suggests that TGF-β signaling in proliferating NSCs in the early postnatal DG is cell autonomous (Figures 1E and 1H). Together, these studies suggest a conserved role of the TGF-β superfamily in regulating quiescence of NSCs in the DG with autocrine TGF-β signaling in early postnatal stages and paracrine BMP signaling in adulthood.

Unlike many previous studies involving m^{6}A-related mechanisms that often attribute the functional phenotypes to one or a few individual m^{6}A targets,[35,38] our study uncovers a distinct molecular logic, with an example of m^{6}A-mediated convergent epitranscriptomic co-regulation of multiple components of a single signaling pathway to regulate NSCs. Multiple components of the TGF-β-signaling pathway were m^{6}A tagged and regulated by YTHDF2-mediated mRNA decay, from TGF-β ligands (*Tgfb2* and *Tgfb3*), TGF-β maturation and activation factors (*Furin* and *Thbs1*), TGF-β receptor (*Tgfbr2*), and downstream SMAD-binding transcription regulators (*Runx1*, *Yap1*, and *Tgif1*) to TGF-β-signaling modulators (*Hras1*, *Itga3*, and *Tsku*) (Figure 2I). Although the effect of m^{6}A- and YTHDF2-dependent mRNA decay on each individual component might be modest, the convergent effect on TGF-β signaling could be robust, as shown by strong upregulation of TGF-β signaling in *Ythdf2* cKO and *Mettl14* cKO NSCs (Figures 3G, 3H, S3L, and S3M). This mode of tuning a key signaling pathway through epitranscriptomic co-regulation of its multiple components simultaneously can offer several advantages to achieve both robustness and specificity of signaling. First, the mRNA level of a single component of a key signaling pathway could be dynamic and fluctuating,[64] but controlling multiple components at the same time can lead to stable and robust regulation of the key signaling pathway to reliably regulate cellular function. Second, there are numerous crosstalks between major signaling pathways and one component could also be involved in multiple pathways.[65] For example, Yap1 binds to SMAD2/3 and mediates their nuclear translocation, thus regulating TGF-β-SMAD signaling,[52,53] while Yap1 is also the main effector of the Hippo tumor-suppressor pathway.[66] The converged epitranscriptomic co-regulation of multiple components in the same pathway, with a modest impact on each individual component, can ensure the specificity of the signaling with minimal perturbation of parallel pathways that share common mediators.

The epitranscriptomic co-regulation of multiple components of one signaling pathway necessitates the stability of the RNA modification and downstream signaling machinery. Notably, YTHDF2, the m^{6}A reader protein involved in m^{6}A-mediated mRNA decay, is also m^{6}A tagged and bound by the YTHDF2 protein itself (Figures 2K and 2L). Moreover, deletion of exon 4 of *Ythdf2* did not induce nonsense-mediated decay of the remnant *Ythdf2* mRNA but robustly enhanced its expression (Figure S2H), at least partially due to its slower decay in *Ythdf2* cKO NSCs. This result suggests an m^{6}A-mediated feedback regulatory loop between *Ythdf2* mRNA and YTHDF2 protein, rendering a stable level of YTHDF2 protein and preventing its overexpression. Such regulation highlights an example of a regulatory loop from mRNA to protein that binds its own mRNA with m^{6}A modifications to promote mRNA decay and stabilize its total protein level, a paradigm that broadens the central dogma of genetic information flow from DNA to RNA to protein.[67]

Limitations of the study

First, the mechanisms by which m^{6}A methyltransferases and YTHDF2 specifically targets those components of the TGF-β-signaling pathway identified here remain unresolved, and how such specificity for m^{6}A modification and reader recognition is achieved is a general question for the whole epitranscriptomic field.[68,69] Second, our study focuses on the role of

(D–F) A schematic diagram of the experimental design of the administration of SB-431542 (10 mg/kg) (D), sample confocal images of staining in the upper blade of DG at P7 (E; scale bars: 20 μm), and quantifications (F). Red arrows indicate MCM2$^+$YFP$^+$Nestin$^+$ NSCs (E). The same data for WT and cKO without treatment as in Figure 1D are replotted for comparison. Values represent mean ± SEM (n = 5/WT; 5/cKO; 5/WT + SB-431542; 6/cKO + SB-431542; ns: $p > 0.05$; $^{**}p < 0.01$; $^{***}p < 0.001$; one-way ANOVA).

(G–I) A schematic diagram of the experimental design of the long-term administration of DMSO or SB-431542 in CD-1® IGS (CD1) mice (G), sample confocal images of staining in the upper blade of DG at P14 (H; scale bars: 10 μm), and quantifications (I). Stars indicate MCM2$^+$Hopx$^+$Nestin$^+$ NSCs (H). Values represent mean ± SEM (n = 5; $^{***}p < 0.001$; Student's t test).

See also Figure S4.

YTHDF2-mediated mRNA decay in the early postnatal stages, yet whether this pathway continues to regulate NSC quiescence maintenance in the adult DG and the potential consequence of developmental dysregulation of this pathway in adults remains to be investigated. Third, whether other m^{6}A readers, such as members of the *Igf2bp* family, which promote mRNA stability[70] and exhibit a similar pattern of dynamic expression as *Ythdf2* in NSCs from E15, P3 to adult (Figure S1A), or other members of the TGF-β super family, such as BMPs, regulate quiescence acquisition of NSCs in the early postnatal DG is an interesting question for future studies.

RESOURCE AVAILABILITY

Lead contact

Further information and requests for resources and reagents should be directed to and will be fulfilled by the lead contact, Hongjun Song (shongjun@pennmedicine.upenn.edu).

Materials availability

All unique/stable reagents generated in this study are available from the lead contact, Hongjun Song (shongjun@pennmedicine.upenn.edu), with a completed Materials Transfer Agreement.

Data and code availability

The RNA-seq, m^{6}A-seq, and YTHDF-RIP-seq datasets reported in this study are deposited in NCBI GEO: GSE266096. No original code was generated in this study.

ACKNOWLEDGMENTS

We thank members of the Song and Ming laboratories for discussion, Kimberly M. Christian for comments, and J.G. Schnoll, B. Temsamrit, E. LaNoce, A. Garcia, A. Angelucci, and G. Alepa for technical support and lab coordination. This work was supported by grants from the National Institutes of Health (R35NS116843 to H.S., R35NS097370 to G.-l.M., and RM1HG008935 to C.H. and H.S.) and Dr. Miriam and Sheldon G. Adelson Medical Research Foundation (to G.-l.M., R.K., and D.H.G.).

AUTHOR CONTRIBUTIONS

F.Z. led the project and collected and analyzed data. Y.F. performed some of the immunohistology experiments. D.J.-C., Y. Shen, and Y. Sun analyzed some of the sequencing data. T.Z. and Z.Z. constructed the plasmids and prepared the lentivirus. Q.W., R.K., and D.H.G. performed the sequencing. C.H. provided *Mettl14*$^{f/f}$ and *Ythdf2*$^{f/f}$ mice. F.Z., G.-l.M., and H.S. conceived the project and experimental design and wrote the manuscript, with comments from all authors.

DECLARATION OF INTERESTS

G.-l.M. is a member of the editorial board of *Cell Stem Cell*.

STAR★METHODS

Detailed methods are provided in the online version of this paper and include the following:

SUPPLEMENTAL INFORMATION

Supplemental information can be found online at https://doi.org/10.1016/j.stem.2024.10.002.

Received: May 23, 2024
Revised: August 26, 2024
Accepted: October 2, 2024
Published: October 29, 2024

REFERENCES

1. Gage, F.H. (2000). Mammalian neural stem cells. Science *287*, 1433–1438.
2. Ming, G.L., and Song, H. (2011). Adult neurogenesis in the mammalian brain: significant answers and significant questions. Neuron *70*, 687–702. https://doi.org/10.1016/j.neuron.2011.05.001.
3. Christian, K.M., Song, H., and Ming, G.L. (2014). Functions and dysfunctions of adult hippocampal neurogenesis. Annu. Rev. Neurosci. *37*, 243–262. https://doi.org/10.1146/annurev-neuro-071013-014134.
4. Anacker, C., and Hen, R. (2017). Adult hippocampal neurogenesis and cognitive flexibility - linking memory and mood. Nat. Rev. Neurosci. *18*, 335–346. https://doi.org/10.1038/nrn.2017.45.
5. Kempermann, G., Song, H., and Gage, F.H. (2015). Neurogenesis in the adult hippocampus. Cold Spring Harb. Perspect. Biol. *7*, a018812. https://doi.org/10.1101/cshperspect.a018812.
6. Denoth-Lippuner, A., and Jessberger, S. (2021). Formation and integration of new neurons in the adult hippocampus. Nat. Rev. Neurosci. *22*, 223–236. https://doi.org/10.1038/s41583-021-00433-z.
7. Eisch, A.J., and Petrik, D. (2012). Depression and hippocampal neurogenesis: a road to remission? Science *338*, 72–75. https://doi.org/10.1126/science.1222941.
8. Yun, S., Reynolds, R.P., Masiulis, I., and Eisch, A.J. (2016). Re-evaluating the link between neuropsychiatric disorders and dysregulated adult neurogenesis. Nat. Med. *22*, 1239–1247. https://doi.org/10.1038/nm.4218.
9. Terreros-Roncal, J., Moreno-Jiménez, E.P., Flor-García, M., Rodríguez-Moreno, C.B., Trinchero, M.F., Cafini, F., Rábano, A., and Llorens-Martín, M. (2021). Impact of neurodegenerative diseases on human adult hippocampal neurogenesis. Science *374*, 1106–1113. https://doi.org/10.1126/science.abl5163.
10. Zhou, Y., Su, Y., Li, S., Kennedy, B.C., Zhang, D.Y., Bond, A.M., Sun, Y., Jacob, F., Lu, L., Hu, P., et al. (2022). Molecular landscapes of human hippocampal immature neurons across lifespan. Nature *607*, 527–533. https://doi.org/10.1038/s41586-022-04912-w.
11. Berg, D.A., Su, Y., Jimenez-Cyrus, D., Patel, A., Huang, N., Morizet, D., Lee, S., Shah, R., Ringeling, F.R., Jain, R., et al. (2019). A common embryonic origin of stem cells drives developmental and adult neurogenesis. Cell *177*, 654–668.e15. https://doi.org/10.1016/j.cell.2019.02.010.
12. Bond, A.M., Ming, G.L., and Song, H. (2021). Ontogeny of adult neural stem cells in the mammalian brain. Curr. Top. Dev. Biol. *142*, 67–98. https://doi.org/10.1016/bs.ctdb.2020.11.002.
13. Berg, D.A., Bond, A.M., Ming, G.L., and Song, H. (2018). Radial glial cells in the adult dentate gyrus: what are they and where do they come from? F1000Res *7*, 277. https://doi.org/10.12688/f1000research.12684.1.
14. Urbán, N., Blomfield, I.M., and Guillemot, F. (2019). Quiescence of adult mammalian neural stem cells: A highly regulated rest. Neuron *104*, 834–848. https://doi.org/10.1016/j.neuron.2019.09.026.

15. Calatayud-Baselga, I., Casares-Crespo, L., Franch-Ibáñez, C., Guijarro-Nuez, J., Sanz, P., and Mira, H. (2023). Autophagy drives the conversion of developmental neural stem cells to the adult quiescent state. Nat. Commun. *14*, 7541. https://doi.org/10.1038/s41467-023-43222-1.

16. Jimenez-Cyrus, D., Adusumilli, V.S., Stempel, M.H., Maday, S., Ming, G.L., Song, H., and Bond, A.M. (2024). Molecular cascade reveals sequential milestones underlying hippocampal neural stem cell development into an adult state. Cell Rep. *43*, 114339. https://doi.org/10.1016/j.celrep.2024.114339.

17. Zhang, F., Yoon, K., Kim, N.S., Ming, G.L., and Song, H. (2023). Cell-autonomous and non-cell-autonomous roles of NKCC1 in regulating neural stem cell quiescence in the hippocampal dentate gyrus. Stem Cell Rep. *18*, 1468–1481. https://doi.org/10.1016/j.stemcr.2023.05.021.

18. Derynck, R., and Zhang, Y.E. (2003). Smad-dependent and Smad-independent pathways in TGF-beta family signalling. Nature *425*, 577–584. https://doi.org/10.1038/nature02006.

19. Mira, H., Andreu, Z., Suh, H., Lie, D.C., Jessberger, S., Consiglio, A., San Emeterio, J., Hortigüela, R., Marqués-Torrejón, M.A., Nakashima, K., et al. (2010). Signaling through BMPR-IA regulates quiescence and long-term activity of neural stem cells in the adult hippocampus. Cell Stem Cell *7*, 78–89. https://doi.org/10.1016/j.stem.2010.04.016.

20. Buckwalter, M.S., Yamane, M., Coleman, B.S., Ormerod, B.K., Chin, J.T., Palmer, T., and Wyss-Coray, T. (2006). Chronically increased transforming growth factor-beta1 strongly inhibits hippocampal neurogenesis in aged mice. Am. J. Pathol. *169*, 154–164. https://doi.org/10.2353/ajpath.2006.051272.

21. Wachs, F.P., Winner, B., Couillard-Despres, S., Schiller, T., Aigner, R., Winkler, J., Bogdahn, U., and Aigner, L. (2006). Transforming growth factor-beta1 is a negative modulator of adult neurogenesis. J. Neuropathol. Exp. Neurol. *65*, 358–370. https://doi.org/10.1097/01.jnen.0000218444.53405.f0.

22. Hiew, L.F., Poon, C.H., You, H.Z., and Lim, L.W. (2021). TGF-beta/Smad signalling in neurogenesis: implications for neuropsychiatric diseases. Cells *10*, 1382. https://doi.org/10.3390/cells10061382.

23. Dias, J.M., Alekseenko, Z., Applequist, J.M., and Ericson, J. (2014). Tgfbeta signaling regulates temporal neurogenesis and potency of neural stem cells in the CNS. Neuron *84*, 927–939. https://doi.org/10.1016/j.neuron.2014.10.033.

24. Li, M., Zhao, X., Wang, W., Shi, H., Pan, Q., Lu, Z., Perez, S.P., Suganthan, R., He, C., Bjørås, M., et al. (2018). Ythdf2-mediated m(6)A mRNA clearance modulates neural development in mice. Genome Biol. *19*, 69. https://doi.org/10.1186/s13059-018-1436-y.

25. Yoon, K.J., Ringeling, F.R., Vissers, C., Jacob, F., Pokrass, M., Jimenez-Cyrus, D., Su, Y., Kim, N.S., Zhu, Y., Zheng, L., et al. (2017). Temporal control of mammalian cortical neurogenesis by m(6)A methylation. Cell *171*, 877–889.e17. https://doi.org/10.1016/j.cell.2017.09.003.

26. Wang, Y., Li, Y., Yue, M., Wang, J., Kumar, S., Wechsler-Reya, R.J., Zhang, Z., Ogawa, Y., Kellis, M., Duester, G., et al. (2018). N(6)-methyladenosine RNA modification regulates embryonic neural stem cell self-renewal through histone modifications. Nat. Neurosci. *21*, 195–206. https://doi.org/10.1038/s41593-017-0057-1.

27. Zhao, B.S., Roundtree, I.A., and He, C. (2017). Post-transcriptional gene regulation by mRNA modifications. Nat. Rev. Mol. Cell Biol. *18*, 31–42. https://doi.org/10.1038/nrm.2016.132.

28. Zhang, F., Ignatova, V.V., Ming, G.L., and Song, H. (2024). Advances in brain epitranscriptomics research and translational opportunities. Mol. Psychiatry *29*, 449–463. https://doi.org/10.1038/s41380-023-02339-x.

29. Morais, P., Adachi, H., and Yu, Y.T. (2021). The critical contribution of pseudouridine to mRNA COVID-19 vaccines. Front. Cell Dev. Biol. *9*, 789427. https://doi.org/10.3389/fcell.2021.789427.

30. Zaccara, S., Ries, R.J., and Jaffrey, S.R. (2019). Reading, writing and erasing mRNA methylation. Nat. Rev. Mol. Cell Biol. *20*, 608–624. https://doi.org/10.1038/s41580-019-0168-5.

31. Jiang, X., Liu, B., Nie, Z., Duan, L., Xiong, Q., Jin, Z., Yang, C., and Chen, Y. (2021). The role of m6A modification in the biological functions and diseases. Signal Transduct. Target. Ther. *6*, 74. https://doi.org/10.1038/s41392-020-00450-x.

32. Wang, X., Lu, Z., Gomez, A., Hon, G.C., Yue, Y., Han, D., Fu, Y., Parisien, M., Dai, Q., Jia, G., et al. (2014). N6-methyladenosine-dependent regulation of messenger RNA stability. Nature *505*, 117–120. https://doi.org/10.1038/nature12730.

33. Zaccara, S., and Jaffrey, S.R. (2020). A Unified Model for the function of YTHDF proteins in regulating m(6)A-modified mRNA. Cell *181*, 1582–1595.e18. https://doi.org/10.1016/j.cell.2020.05.012.

34. Shi, H., Zhang, X., Weng, Y.L., Lu, Z., Liu, Y., Lu, Z., Li, J., Hao, P., Zhang, Y., Zhang, F., et al. (2018). m(6)A facilitates hippocampus-dependent learning and memory through YTHDF1. Nature *563*, 249–253. https://doi.org/10.1038/s41586-018-0666-1.

35. Zhuang, M., Geng, X., Han, P., Che, P., Liang, F., Liu, C., Yang, L., Yu, J., Zhang, Z., Dong, W., et al. (2023). YTHDF2 in dentate gyrus is the m(6)A reader mediating m(6)A modification in hippocampus-dependent learning and memory. Mol. Psychiatry *28*, 1679–1691. https://doi.org/10.1038/s41380-023-01953-z.

36. Meyer, K.D., Saletore, Y., Zumbo, P., Elemento, O., Mason, C.E., and Jaffrey, S.R. (2012). Comprehensive analysis of mRNA methylation reveals enrichment in 3′ UTRs and near stop codons. Cell *149*, 1635–1646. https://doi.org/10.1016/j.cell.2012.05.003.

37. Li, Z., Qian, P., Shao, W., Shi, H., He, X.C., Gogol, M., Yu, Z., Wang, Y., Qi, M., Zhu, Y., et al. (2018). Suppression of m(6)A reader Ythdf2 promotes hematopoietic stem cell expansion. Cell Res. *28*, 904–917. https://doi.org/10.1038/s41422-018-0072-0.

38. Chen, J., Zhang, Y.C., Huang, C., Shen, H., Sun, B., Cheng, X., Zhang, Y.J., Yang, Y.G., Shu, Q., Yang, Y., et al. (2019). m(6)A regulates neurogenesis and neuronal development by modulating histone methyltransferase Ezh2. Genomics Proteomics Bioinformatics *17*, 154–168. https://doi.org/10.1016/j.gpb.2018.12.007.

39. Shin, J., Berg, D.A., Zhu, Y., Shin, J.Y., Song, J., Bonaguidi, M.A., Enikolopov, G., Nauen, D.W., Christian, K.M., Ming, G.L., et al. (2015). Single-Cell RNA-Seq with Waterfall Reveals Molecular Cascades underlying Adult Neurogenesis. Cell Stem Cell *17*, 360–372. https://doi.org/10.1016/j.stem.2015.07.013.

40. Wharton, S.B., Chan, K.K., Anderson, J.R., Stoeber, K., and Williams, G.H. (2001). Replicative Mcm2 protein as a novel proliferation marker in oligodendrogliomas and its relationship to Ki67 labelling index, histological grade and prognosis. Neuropathol. Appl. Neurobiol. *27*, 305–313. https://doi.org/10.1046/j.0305-1846.2001.00333.x.

41. Micaelli, M., Dalle Vedove, A., Cerofolini, L., Vigna, J., Sighel, D., Zaccara, S., Bonomo, I., Poulentzas, G., Rosatti, E.F., Cazzanelli, G., et al. (2022). Small-molecule ebselen binds to YTHDF proteins interfering with the recognition of N (6)-Methyladenosine-Modified RNAs. ACS Pharmacol. Transl. Sci. *5*, 872–891. https://doi.org/10.1021/acsptsci.2c00008.

42. Liu, J., Yue, Y., Han, D., Wang, X., Fu, Y., Zhang, L., Jia, G., Yu, M., Lu, Z., Deng, X., et al. (2014). A METTL3-METTL14 complex mediates mammalian nuclear RNA N6-adenosine methylation. Nat. Chem. Biol. *10*, 93–95. https://doi.org/10.1038/nchembio.1432.

43. Akhurst, R.J., and Hata, A. (2012). Targeting the TGFbeta signalling pathway in disease. Nat. Rev. Drug Discov. *11*, 790–811. https://doi.org/10.1038/nrd3810.

44. Massagué, J., and Sheppard, D. (2023). TGF-beta signaling in health and disease. Cell *186*, 4007–4037. https://doi.org/10.1016/j.cell.2023.07.036.

45. Gorbacheva, A.M., Uvarova, A.N., Ustiugova, A.S., Bhattacharyya, A., Korneev, K.V., Kuprash, D.V., and Mitkin, N.A. (2021). EGR1 and RXRA transcription factors link TGF-beta pathway and CCL2 expression in triple negative breast cancer cells. Sci. Rep. *11*, 14120. https://doi.org/10.1038/s41598-021-93561-6.

46. Datto, M.B., Li, Y., Panus, J.F., Howe, D.J., Xiong, Y., and Wang, X.F. (1995). Transforming growth factor beta induces the cyclin-dependent

kinase inhibitor p21 through a p53-independent mechanism. Proc. Natl. Acad. Sci. USA *92*, 5545–5549. https://doi.org/10.1073/pnas.92.12.5545.

47. Nakashima, H., Tsujimura, K., Irie, K., Ishizu, M., Pan, M., Kameda, T., and Nakashima, K. (2018). Canonical TGF-beta signaling negatively regulates neuronal morphogenesis through TGIF/Smad complex-mediated CRMP2 suppression. J. Neurosci. *38*, 4791–4810. https://doi.org/10.1523/JNEUROSCI.2423-17.2018.
48. Dubois, C.M., Blanchette, F., Laprise, M.H., Leduc, R., Grondin, F., and Seidah, N.G. (2001). Evidence that furin is an authentic transforming growth factor-beta1-converting enzyme. Am. J. Pathol. *158*, 305–316. https://doi.org/10.1016/s0002-9440(10)63970-3.
49. Farberov, S., Basavaraja, R., and Meidan, R. (2019). Thrombospondin-1 at the crossroads of corpus luteum fate decisions. Reproduction *157*, R73–R83. https://doi.org/10.1530/REP-18-0530.
50. Ito, Y., and Miyazono, K. (2003). RUNX transcription factors as key targets of TGF-beta superfamily signaling. Curr. Opin. Genet. Dev. *13*, 43–47. https://doi.org/10.1016/s0959-437x(03)00007-8.
51. Guo, Z., Liu, X., Zhao, S., Sun, F., Ren, W., and Ma, M. (2023). RUNX1 promotes liver fibrosis progression through regulating TGF-beta signalling. Int. J. Exp. Pathol. *104*, 188–198. https://doi.org/10.1111/iep.12474.
52. Nakamura, R., Hiwatashi, N., Bing, R., Doyle, C.P., and Branski, R.C. (2021). Concurrent YAP/TAZ and SMAD signaling mediate vocal fold fibrosis. Sci. Rep. *11*, 13484. https://doi.org/10.1038/s41598-021-92871-z.
53. Varelas, X., Samavarchi-Tehrani, P., Narimatsu, M., Weiss, A., Cockburn, K., Larsen, B.G., Rossant, J., and Wrana, J.L. (2010). The Crumbs complex couples cell density sensing to Hippo-dependent control of the TGF-beta-SMAD pathway. Dev. Cell *19*, 831–844. https://doi.org/10.1016/j.devcel.2010.11.012.
54. Wotton, D., Knoepfler, P.S., Laherty, C.D., Eisenman, R.N., and Massague, J. (2001). The Smad transcriptional corepressor TGIF recruits mSin3. Cell Growth Differ. *12*, 457–463.
55. Wotton, D., Lo, R.S., Lee, S., and Massagué, J. (1999). A Smad transcriptional corepressor. Cell *97*, 29–39. https://doi.org/10.1016/s0092-8674(00)80712-6.
56. Liu, S., Iaria, J., Simpson, R.J., and Zhu, H.J. (2018). Ras enhances TGF-beta signaling by decreasing cellular protein levels of its type II receptor negative regulator SPSB1. Cell Commun. Signal. *16*, 10. https://doi.org/10.1186/s12964-018-0223-4.
57. Reynolds, L.E., Conti, F.J., Silva, R., Robinson, S.D., Iyer, V., Rudling, R., Cross, B., Nye, E., Hart, I.R., Dipersio, C.M., et al. (2008). alpha3beta1 integrin-controlled Smad7 regulates reepithelialization during wound healing in mice. J. Clin. Invest. *118*, 965–974. https://doi.org/10.1172/JCI33538.
58. Niimori, D., Kawano, R., Felemban, A., Niimori-Kita, K., Tanaka, H., Ihn, H., and Ohta, K. (2012). Tsukushi controls the hair cycle by regulating TGF-beta1 signaling. Dev. Biol. *372*, 81–87. https://doi.org/10.1016/j.ydbio.2012.08.030.
59. Caraci, F., Gulisano, W., Guida, C.A., Impellizzeri, A.A.R., Drago, F., Puzzo, D., and Palmeri, A. (2015). A key role for TGF-beta1 in hippocampal synaptic plasticity and memory. Sci. Rep. *5*, 11252. https://doi.org/10.1038/srep11252.
60. Palazuelos, J., Klingener, M., and Aguirre, A. (2014). TGFbeta signaling regulates the timing of CNS myelination by modulating oligodendrocyte progenitor cell cycle exit through SMAD3/4/FoxO1/Sp1. J. Neurosci. *34*, 7917–7930. https://doi.org/10.1523/JNEUROSCI.0363-14.2014.
61. Ronaldson, P.T., Demarco, K.M., Sanchez-Covarrubias, L., Solinsky, C.M., and Davis, T.P. (2009). Transforming growth factor-beta signaling alters substrate permeability and tight junction protein expression at the blood-brain barrier during inflammatory pain. J. Cereb. Blood Flow Metab. *29*, 1084–1098. https://doi.org/10.1038/jcbfm.2009.32.
62. Ben-Ari, Y., Khalilov, I., Kahle, K.T., and Cherubini, E. (2012). The GABA excitatory/inhibitory shift in brain maturation and neurological disorders. Neuroscientist *18*, 467–486. https://doi.org/10.1177/1073858412438697.
63. Komatsu, M., Waguri, S., Chiba, T., Murata, S., Iwata, J., Tanida, I., Ueno, T., Koike, M., Uchiyama, Y., Kominami, E., et al. (2006). Loss of autophagy in the central nervous system causes neurodegeneration in mice. Nature *441*, 880–884. https://doi.org/10.1038/nature04723.
64. Raj, A., and van Oudenaarden, A. (2008). Nature, nurture, or chance: stochastic gene expression and its consequences. Cell *135*, 216–226. https://doi.org/10.1016/j.cell.2008.09.050.
65. Luo, K. (2017). Signaling cross talk between TGF-beta/Smad and other signaling pathways. Cold Spring Harb. Perspect. Biol. *9*, a022137. https://doi.org/10.1101/cshperspect.a022137.
66. Piccolo, S., Dupont, S., and Cordenonsi, M. (2014). The biology of YAP/TAZ: hippo signaling and beyond. Physiol. Rev. *94*, 1287–1312. https://doi.org/10.1152/physrev.00005.2014.
67. Lin, Z., Zhao, S., Li, X., Miao, Z., Cao, J., Chen, Y., Shi, Z., Zhang, J., Wang, D., Chen, S., et al. (2023). Cathepsin B S-nitrosylation promotes ADAR1-mediated editing of its own mRNA transcript via an ADD1/MATR3 regulatory axis. Cell Res. *33*, 546–561. https://doi.org/10.1038/s41422-023-00812-4.
68. He, P.C., Wei, J., Dou, X., Harada, B.T., Zhang, Z., Ge, R., Liu, C., Zhang, L.S., Yu, X., Wang, S., et al. (2023). Exon architecture controls mRNA m(6)A suppression and gene expression. Science *379*, 677–682. https://doi.org/10.1126/science.abj9090.
69. Huang, H., Weng, H., Zhou, K., Wu, T., Zhao, B.S., Sun, M., Chen, Z., Deng, X., Xiao, G., Auer, F., et al. (2019). Histone H3 trimethylation at lysine 36 guides m(6)A RNA modification co-transcriptionally. Nature *567*, 414–419. https://doi.org/10.1038/s41586-019-1016-7.
70. Huang, H., Weng, H., Sun, W., Qin, X., Shi, H., Wu, H., Zhao, B.S., Mesquita, A., Liu, C., Yuan, C.L., et al. (2018). Recognition of RNA N(6)-methyladenosine by IGF2BP proteins enhances mRNA stability and translation. Nat. Cell Biol. *20*, 285–295. https://doi.org/10.1038/s41556-018-0045-z.
71. Zhao, T., Hong, Y., Yan, B., Huang, S., Ming, G.L., and Song, H. (2024). Epigenetic maintenance of adult neural stem cell quiescence in the mouse hippocampus via Setd1a. Nat. Commun. *15*, 5674. https://doi.org/10.1038/s41467-024-50010-y.
72. Matsuda, T., and Cepko, C.L. (2004). Electroporation and RNA interference in the rodent retina in vivo and in vitro. Proc. Natl. Acad. Sci. USA *101*, 16–22. https://doi.org/10.1073/pnas.2235688100.
73. Enomoto, M., Bunge, M.B., and Tsoulfas, P. (2013). A multifunctional neurotrophin with reduced affinity to p75NTR enhances transplanted Schwann cell survival and axon growth after spinal cord injury. Exp. Neurol. *248*, 170–182. https://doi.org/10.1016/j.expneurol.2013.06.013.
74. Truitt, J.M., Blednov, Y.A., Benavidez, J.M., Black, M., Ponomareva, O., Law, J., Merriman, M., Horani, S., Jameson, K., Lasek, A.W., et al. (2016). Inhibition of IKKbeta reduces ethanol consumption in C57BL/6J mice. eNeuro *3*. https://doi.org/10.1523/ENEURO.0256-16.2016.
75. Stewart, S.A., Dykxhoorn, D.M., Palliser, D., Mizuno, H., Yu, E.Y., An, D.S., Sabatini, D.M., Chen, I.S.Y., Hahn, W.C., Sharp, P.A., et al. (2003). Lentivirus-delivered stable gene silencing by RNAi in primary cells. RNA *9*, 493–501. https://doi.org/10.1261/rna.2192803.
76. Kim, Y.S., Kang, E., Makino, Y., Park, S., Shin, J.H., Song, H., Launay, P., and Linden, D.J. (2013). Characterizing the conductance underlying depolarization-induced slow current in cerebellar Purkinje cells. J. Neurophysiol. *109*, 1174–1181. https://doi.org/10.1152/jn.01168.2011.
77. Love, M.I., Huber, W., and Anders, S. (2014). Moderated estimation of fold change and dispersion for RNA-seq data with DESeq2. Genome Biol. *15*, 550. https://doi.org/10.1186/s13059-014-0550-8.
78. Zhou, Y., Zhou, B., Pache, L., Chang, M., Khodabakhshi, A.H., Tanaseichuk, O., Benner, C., and Chanda, S.K. (2019). Metascape provides a biologist-oriented resource for the analysis of systems-level datasets. Nat. Commun. *10*, 1523. https://doi.org/10.1038/s41467-019-09234-6.
79. Dobin, A., Davis, C.A., Schlesinger, F., Drenkow, J., Zaleski, C., Jha, S., Batut, P., Chaisson, M., and Gingeras, T.R. (2013). STAR: ultrafast

universal RNA-seq aligner. Bioinformatics *29*, 15–21. https://doi.org/10.1093/bioinformatics/bts635.

80. Bolger, A.M., Lohse, M., and Usadel, B. (2014). Trimmomatic: a flexible trimmer for Illumina sequence data. Bioinformatics *30*, 2114–2120. https://doi.org/10.1093/bioinformatics/btu170.
81. Tronche, F., Kellendonk, C., Kretz, O., Gass, P., Anlag, K., Orban, P.C., Bock, R., Klein, R., and Schütz, G. (1999). Disruption of the glucocorticoid receptor gene in the nervous system results in reduced anxiety. Nat. Genet. *23*, 99–103. https://doi.org/10.1038/12703.
82. Srinivas, S., Watanabe, T., Lin, C.S., William, C.M., Tanabe, Y., Jessell, T.M., and Costantini, F. (2001). Cre reporter strains produced by targeted insertion of EYFP and ECFP into the ROSA26 locus. BMC Dev. Biol. *1*, 4.
83. Takeda, N., Jain, R., LeBoeuf, M.R., Wang, Q., Lu, M.M., and Epstein, J.A. (2011). Interconversion between intestinal stem cell populations in distinct niches. Science *334*, 1420–1424. https://doi.org/10.1126/science.1213214.
84. Bonaguidi, M.A., Wheeler, M.A., Shapiro, J.S., Stadel, R.P., Sun, G.J., Ming, G.L., and Song, H. (2011). In vivo clonal analysis reveals self-renewing and multipotent adult neural stem cell characteristics. Cell *145*, 1142–1155. https://doi.org/10.1016/j.cell.2011.05.024.
85. De Feo, D., Merlini, A., Brambilla, E., Ottoboni, L., Laterza, C., Menon, R., Srinivasan, S., Farina, C., Garcia Manteiga, J.M., Butti, E., et al. (2017). Neural precursor cell-secreted TGF-beta2 redirects inflammatory monocyte-derived cells in CNS autoimmunity. J. Clin. Invest. *127*, 3937–3953. https://doi.org/10.1172/JCI92387.
86. Zhang, F., Yoon, K., Zhang, D.Y., Kim, N.S., Ming, G.L., and Song, H. (2023). Epitranscriptomic regulation of cortical neurogenesis via Mettl8-dependent mitochondrial tRNA m(3)C modification. Cell Stem Cell *30*, 300–311.e11. https://doi.org/10.1016/j.stem.2023.01.007.
87. Weng, Y.L., Wang, X., An, R., Cassin, J., Vissers, C., Liu, Y., Liu, Y., Xu, T., Wang, X., Wong, S.Z.H., et al. (2018). Epitranscriptomic m(6)A regulation of axon regeneration in the adult mammalian nervous system. Neuron *97*, 313–325.e6. https://doi.org/10.1016/j.neuron.2017.12.036.
88. Hagemann-Jensen, M., Ziegenhain, C., and Sandberg, R. (2022). Scalable single-cell RNA sequencing from full transcripts with Smart-seq3xpress. Nat. Biotechnol. *40*, 1452–1457. https://doi.org/10.1038/s41587-022-01311-4.
89. Batista, P.J., Molinie, B., Wang, J., Qu, K., Zhang, J., Li, L., Bouley, D.M., Lujan, E., Haddad, B., Daneshvar, K., et al. (2014). m(6)A RNA modification controls cell fate transition in mammalian embryonic stem cells. Cell Stem Cell *15*, 707–719. https://doi.org/10.1016/j.stem.2014.09.019.

STAR★METHODS

KEY RESOURCES TABLE

REAGENT or RESOURCE	SOURCE	IDENTIFIER
Antibodies		
Chicken polyclonal anti-Nestin	Aves labs	Cat#NES; RRID: AB_2314882
Goat polyclonal anti-GFP	Rockland	Cat#600101215; RRID: AB 11181883
Goat polyclonal anti-SOX2	R&D system	Cat#AF2018; RRID: AB_355110
Goat polyclonal anti-TGFBRII	NOVUS BIOLOGICAL	Cat#AF-241-SP; RRID: AB_354416
Mouse monoclonal anti-Ki67	BD Biosciences	Cat#550609; RRID: AB_393778
Mouse monoclonal anti-MCM2	BD Biosciences	Cat#610701; RRID: AB_398024
Mouse monoclonal anti-β-actin	Thermo Fisher Scientific	Cat#AM4302; RRID: AB_2536382
Rabbit monoclonal anti-GAPDH	Cell Signaling Technology	Cat#2118; RRID: AB_561053
Rabbit monoclonal anti-m^{6}A	EMSCO/Fisher	Cat#ABE572; RRID: AB_2892213
Rabbit monoclonal anti-Phospho-SMAD2 (Ser465/467)	Cell Signaling Technology	Cat#3108s; RRID: AB_490941
Rabbit monoclonal anti-Prox1	ABCAM	Cat#ab199359; RRID: AB_2868427
Rabbit monoclonal anti-SMAD2	Cell Signaling Technology	Cat#5339S; RRID: AB_10626777
Rabbit polyclonal anti-Cleaved caspase3	Cell Signaling Technology	Cat#9661; RRID: AB_2341188
Rabbit polyclonal anti-Hopx	Proteintech	Cat#11419-1-1AP; RRID: AB_10693525
Rabbit polyclonal anti-YTHDF2	Aviva systems biology	Cat#ARP67917_P050; RRID: AB_2861185
Rat polyclonal anti-HA	Roche	Cat#11867423001; RRID: AB_390918
Donkey polyclonal anti-Goat IgG (H+L) AffiniPure Secondary Antibody, Alexa Fluor 488	Jackson ImmunoResearch	Cat#705-545-147; RRID: AB_2336933
Donkey polyclonal anti-Goat IgG (H+L) AffiniPure Secondary Antibody, Cy5	Jackson ImmunoResearch	Cat#705-175-147 RRID: AB_2340415
Donkey polyclonal anti-Mouse IgG (H+L) AffiniPure Secondary Antibody, Alexa Fluor 488	Jackson ImmunoResearch	Cat#715-545-151; RRID: AB_2341099
Donkey polyclonal anti-Mouse IgG (H+L) AffiniPure Secondary Antibody, Cy3	Jackson ImmunoResearch	Cat#715-165-151; RRID: AB_2315777
Donkey polyclonal anti-Mouse IgG (H+L) AffiniPure Secondary Antibody, Dylight 405	Jackson ImmunoResearch	Cat#715-475-151; RRID: AB_2340840
Donkey polyclonal anti-Rabbit IgG (H+L) AffiniPure Secondary Antibody, Alexa Fluor 488	Jackson ImmunoResearch	Cat#711-545-152; RRID: AB_2313584
Donkey polyclonal anti-Rabbit IgG (H+L) AffiniPure Secondary Antibody, Cy3	Jackson ImmunoResearch	Cat#711-165-152; RRID: AB_2307443
Donkey polyclonal anti-Rabbit IgG (H+L) AffiniPure Secondary Antibody, Cy5	Jackson ImmunoResearch	Cat#711-175-152; RRID: AB_2340607
Donkey polyclonal anti-Rat IgG (H+L) AffiniPure Secondary Antibody, Cy5	Jackson ImmunoResearch	Cat#112-175-143; RRID: AB_2338263
Donkey polyclonal anti-Chicken IgY (IgG, H+L) AffiniPure Secondary Antibody, Cy3	Jackson ImmunoResearch	Cat#703-165-155; RRID: AB_2340363
Rabbit IgG	Cell Signaling Technology	Cat#2729S; RRID: AB_1031062
Anti-mouse IgG, HRP-linked Antibody	Cell Signaling Technology	Cat#7076, RRID: AB_330924
Anti-rabbit IgG, HRP-linked Antibody	Cell Signaling Technology	Cat#7074, RRID:AB_2099233
Anti-Goat IgG, HRP-linked Antibody	Cell Signaling Technology	N/A
Bacterial and virus strains		
Lenti-pLV-CMV-GFP	Zhao et al.[71]	N/A
Lenti-pLV-CMV-Cre-GFP	Zhao et al.[71]	N/A

(*Continued on next page*)

Continued

REAGENT or RESOURCE	SOURCE	IDENTIFIER
Chemicals, peptides, and recombinant proteins		
0.05% (W/V) Trypsin-EDTA	Corning	Cat#MT25052CI
Actinomycin D	Sigma-Aldrich	Cat#A1410
Advantage UltraPure PCR deoxynucleotide mix (10mM each dNTP)	Takara Bio	Cat#639125
AMPure XP beads	Beckman Coulter	Cat#A63880
Aqua-Mount Mounting Medium	EMSCO/FISHER	Cat#NC9428056
B-27® Supplement	Gibco	Cat#17504044
Blue Protein Loading sample buffer	New England Biolabs	Cat#B7703S
Bovine Serum Albumin (BSA)	VWR Chemicals	Cat#VWRV0332-
Chloroform	Sigma-Aldrich	Cat#C2432
cOmplete, Mini, EDTA-free Protease Inhibitor Cocktail	Sigma-Aldrich	Cat#11836170001
Corn oil	Sigma-Aldrich	Cat#C8267
DAPI	BD Biosciences	Cat#564907
DirectPCR reagent	Fisher Scientific	Cat#NC9724951
DMSO	Sigma-Aldrich	Cat#D2650
Dulbecco's Modification of Eagle's Medium (DMEM)	Corning	Cat#10-013
Dulbecco's Modified Eagle Medium/ Nutrient Mixture F-12 (DMEM/F-12)	Gibco	Cat#11330057
Dulbecco's Phosphate-Buffered Saline (DPBS)	Corning	Cat#14190250
Ebselen	Sigma	Cat#E3520
EdU	Thermo Fisher Scientific	Cat#E10187
EZ-Tn5 Transposase	Lucigen	Cat#TNP92110
Fast SYBR Green Master Mix	Thermo Fisher Scientific	Cat#4385612
Fetal Bovine Serum (FBS)	Corning	Cat#35-010-CV
Formaldehyde, 16%, methanol free, Ultra Pure	Polysciences	Cat#18814-10
GlutaMAX supplement	GIBCO	Cat#35050061
GTP	Thermo Fisher Scientific	Cat#R1461
Human EGF	Peprotech	Cat#AF-100-15
IGEPAL CA-630	Sigma-Aldrich	Cat#I8896
KAPA HiFi Hotstart Readymix	Emsco/Fisher	Cat#KK2601
LipoD293 transfection reagent	Emsco/Fisher	Cat#SL100668
Lipofectamine Stem transfection reagent	Emsco/Fisher	Cat#STEM00001
MagnaBind™ Protein A Beads	Thermo Fisher Scientific	Cat#21348
Maxima H RT enzyme	Thermo Fisher Scientific	Cat#EP0753
N-2 Supplement (100X)	Thermo Fisher Scientific	Cat#17502048
N6-Methyladenosine compound	Sigma-Aldrich	Cat#M2780
Nuclease-Free Water (not DEPC-Treated)	Thermo Fisher Scientific	Cat#AM9937
Penicillin-Streptomycin	Thermo Fisher Scientific	Cat#15140163
PhosSTOP	Sigma-Aldrich	Cat#4906845001
Pierce™ ECL Western Blotting Substrate	Thermo Fisher Scientific	Cat#PI32109
Poly-D-Lysine	Sigma-Aldrich	Cat#P6407
Polyethylene glycol (PEG) solution, 40%	Sigma-Aldrich	Cat# P1458
Protease Inhibitor Cocktail	Sigma-Aldrich	Cat#P8340
Proteinase K	QIAGEN	Cat#19133
Recombinant Human FGF-basic	Peprotech	Cat#100-18B

(*Continued on next page*)

Continued

REAGENT or RESOURCE	SOURCE	IDENTIFIER
RIPA lysis buffer	Thermofisher	Cat#89900
RNase Inhibitor, Murine	New England Biolabs	Cat#M0314S
SB-431542	Sigma-Aldrich	Cat#S4317
SDS (10% w/v)	Fisher Scientific	Cat#50-751-7490
SMARTScribe Reverse Transcriptase	Takara Bio	Cat#639537
StemPro Accutase Cell Dissociation Reagent	Thermo Fisher Scientific	Cat#A1110501
Sucrose	VWR Chemicals	Cat#97061-430
T4 Polynucleotide Kinase	New England Biolabs	Cat#M0289S
Tamoxifen	Sigma-Aldrich	Cat#T5648
Target Retrieval Solution	Agilent Dako	Cat#S1699
Triton X-100	Sigma-Aldrich	Cat#T8787
TRIzol reagent	Thermo Fisher Scientific	Cat#15596026
TWEEN 20	Sigma-Aldrich	Cat#P1379
Critical commercial assays		
Advantage 2 PCR Kit	Takara Bio	Cat#639206
Click-iT Plus EdU Alexa Fluor 647 Imaging Kit	Thermo Fisher Scientific	Cat#C10640
KAPA Library Quantification Kit for Illumina NGS	Kapa Biosystems	Cat#KK4835
mMessage mMachine T7 Ultra kit	Thermo Fisher Scientific	Cat#AM1345
Pierce™ Rapid Gold BCA Protein Assay Kit	Thermo Fisher Scientific	Cat#A53226
Qubit dsDNA HS Assay Kit	Thermo Fisher Scientific	Cat#Q33231
RNA Clean & Concentrator 5	Zymo Research	Cat#R1013
SuperScript III First-Strand Synthesis System	Thermo Fisher Scientific	Cat#18080051
Deposited data		
Raw and analyzed RNA-seq, m^{6}A-Seq and YTHDF2-RIP-seq	This paper	GEO: GSE266096
Experimental models: Organisms/strains		
Mouse: *Ythdf2*$^{flox/flox}$	Li et al.[24]	N/A
Mouse: *Mettl14*$^{flox/flox}$	Yoon et al.[25]	N/A
Mouse: B6.Cg-Tg(Nes-cre)1Kln/J	The Jackson Laboratory	JAX: 003771
Mouse: C57BL/6	Charles River Laboratory	RRID: IMSR_CRL:27
Mouse: Hopx$^{tm2.1(cre/ERT2)Joe}$/J	The Jackson Laboratory	JAX: 017606
Mouse: B6.129X1-Gt(ROSA) 26Sor$^{tm1(EYFP)Cos}$/J	The Jackson Laboratory	JAX: 006148
Oligonucleotides		
The primers and DNA oligos used for qPCR, genotyping and cloning	See Table S1	N/A
Recombinant DNA		
pCAGIG	Matsuda and Cepko[72]	RRID:Addgene_11159
pCAGIG/HA-YTHDF2	This study	N/A
pLV-eGFP	Enomoto et al.[73]	RRID:Addgene_36083
pLV-eGFP-Cre	Truitt et al.[74]	RRID:Addgene_86805
pCMV-VSV-G	Stewart et al.[75]	RRID:Addgene_8454
HIV-1 packaging plasmid Δ8.9	Kim et al.[76]	N/A
Software and algorithms		
Adobe Illustrator CC	Adobe	https://www.adobe.com/products/illustrator.html; RRID: SCR_010279

(*Continued on next page*)

Continued

REAGENT or RESOURCE	SOURCE	IDENTIFIER
Adobe Photoshop CC	Adobe	https://www.adobe.com/products/photoshop.html; RRID: SCR_014199
Bcl2fastq v2.17.1.14	Illumina	https://support.illumina.com/sequencing/sequencing_software/bcl2fastq-conversion-software.html; RRID: SCR_015058
DESeq2 v1.36.0	Love et al.[77]	https://bioconductor.org/packages/release/bioc/html/DESeq2.html; RRID:SCR_015687
GraphPad Prism	GraphPad Software	https://www.graphpad.com/scientific-software/prism/; RRID: SCR_002798
ImageJ	NIH	https://imagej.nih.gov/ij/; RRID: SCR_003070
Imaris	Bitplane	https://imaris.oxinst.com/packages;RRID:SCR_007370
Metascape	Zhou et al.[78]	http://metascape.org/gp/index.html#/main/step1; RRID: SCR_016620
R Project v3.6.0	Open source	https://www.r-project.org/; RRID: SCR_001905
RStudio v1.2.1335	Open source	https://rstudio.com/; RRID: SCR_000432
STAR v2.5.2a	Dobin et al.[79]	https://github.com/alexdobin/STAR; RRID: SCR_015899
Trimmomatic v0.32	Bolger et al.[80]	http://www.usadellab.org/cms/index.php?page=trimmomatic; RRID:SCR_011848
Other		
4-20% Mini-Gel 15-well,	BIO-RAD	Cat#4561096
Amersham Imager 600	GE healthcare	N/A
Charged microscope slides	Fisher Scientific	Cat#22-035813
Forma Steri-Cult CO2 Incubator	Thermo Fisher Scientific	3310
Hamilton Syringe, 25uL	Emsco/Fisher	Cat#6711491
Novaseq 6000 system	Illumina	N/A
Novaseq X+ system	Illumina	N/A
PCR tube strips	Emsco/Fisher	Cat#AB0490
Qubit 3 Fluorimeter	Thermo Fisher Scientific	Cat#Q33216
Sliding frozen microtome	Leica	Cat#SM2010R
StepOnePlus Real-Time PCR	Applied Biosystems	4376592
TB Syringe (26 G x 3/8 in, 1 ml)	BD Biosciences	Cat#309625
Trans-Blot Turbo Mini 0.2 um PVDF Transfer Packs	BIO-RAD	Cat#1704156
Scanning Confocal microscope	Carl Zeiss	Zeiss LSM 780

EXPERIMENTAL MODELS AND STUDY PARTICIPANT DETAILS

Mice

All experimental procedures involving mice were conducted in accordance with protocols approved by the Institutional Animal Care and Use Committee of the University of Pennsylvania. Animals were housed in cages with bedding material and in a 14-hour light/10-hour dark cycle with ad libitum access to food and water. *Ythdf2*$^{f/f}$ and *Mettl14*$^{f/f}$ mice were from Dr. Chuan He's lab at University of Chicago.[25,37] C57BL/6 mice, CD1 mice, *Nestin-Cre* (B6.Cg-Tg$^{(Nes\text{-}cre)1Kln}$/J) transgenic mice (003771), Hopx$^{tm2.1(cre/ERT2)Joe}$/J knock-in mice (017606) and B6.129X1-Gt(ROSA)26Sor$^{tm1(EYFP)Cos}$/J (006148) were all purchased from the Jackson Laboratory.[81–83] *Hopx-CreER*^{T2} mice harbored a tamoxifen-inducible *CreER*^{T2} in-frame fused with the *Hopx* gene, in which injection of tamoxifen at P1 would induce *Cre-loxP*-mediated recombination specifically in Hopx^{+} proliferating NSCs in the DG.[11] *Rosa26*$^{flox\text{-}stop\text{-}flox\text{-}EYFP}$ mice harbored a loxP-flanked STOP sequence followed by the enhanced yellow fluorescent protein gene (eYFP), which was inserted into the Gt(ROSA)26Sor locus, allowing *Cre*-dependent expression of eYFP.[82] The tail tissues of mice were incubated in solution containing directPCR reagent (Fisher Scientific, NC9724951) and 10% proteinase K (QIAGEN, 19133) at 55°C overnight and

subsequently at 85°C for 2 h to isolate the genomic DNA, which was used as templates for genotyping PCR. Genotyping primers for the transgenic mice were obtained from The Jackson Laboratory or self-designed, as listed in Table S1. Both male and female mice were included, and no obvious sex differences were detected in this study.

METHOD DETAILS

Molecular cloning and constructs

C-terminal HA-tagged *Ythdf2* gene was amplified by PCR from complementary DNA (cDNA) of WT hippocampal NSCs and cloned into the pCAGIG vector[72] (Addgene #11159), which were further verified by Sanger sequencing. pLV-eGFP[73] (Addgene #36083) or pLV-EGFP-Cre[74] (Addgene #86805) vector was co-transfected with pCMV-VSV-G[75] (Addgene #8454) and HIV-1 packaging plasmid Δ8.9[76] into HEK293T cells with LipoD293 transfection reagent (Fisher, SL100668) for lentivirus preparation.[71] The sequences of primers used for *Ythdf2* cloning are listed in the key resources table.

Tamoxifen, EdU, and SB-431542 injections

Tamoxifen and EdU injections to mice were performed following the protocols as described previously.[17] A solution of 66.67 mg/mL tamoxifen was made by dissolving 1 g tamoxifen powder (Sigma, T5648) in 2.5 mL ethanol/12.5 mL corn oil (Sigma, C8267) at 37°C with vortexing until fully dissolved.[84] For analysis of NSCs during early postnatal stages, *Hopx-CreER*$^{T2+/-}$*::Ythdf2*$^{+/+}$*::Rosa-YFP*$^{+/-}$ mice (named as Hopx-WT mice) and *Hopx-CreER*$^{T2+/-}$*::Ythdf2*$^{f/f}$*::Rosa-YFP*$^{+/-}$ mice (named as Hopx-cKO mice) at P1 were subcutaneously injected with 10 μL tamoxifen, and analyzed at P7 and P14.

EdU powder (Fisher Scientific, E10187) was dissolved in PBS (10 mg/mL) and incubated on a shaker at 37°C until fully dissolved. For the EdU retaining experiment in early postnatal Hopx-WT and Hopx-cKO mice, mice were first injected with tamoxifen at P1 and then injected with EdU (100 mg/kg) two times at a 6-hour interval at P3 and analyzed 2 hours later or at P14.

SB-431542 (SIGMA, S4317) was dissolved in DMSO (20 mg/mL) and freshly mixed with PBS in a ratio of 1:19. Freshly prepared and well-mixed SB-431542 was injected intraperitoneally into Hopx-WT and Hopx-cKO mice (10 mg/kg) once a day from P4-P7 for four times or into CD1 mice from P4-P14 for 11 times.

Hippocampal and cortical NSC culture, transfection and drug treatment

For primary hippocampal NSC cultures, Nestin-WT, Nestin-cKO, CD1, or *Mettl14*$^{f/f}$ mouse hippocampi at P0.5 were dissected and digested with Trypsin-EDTA at 37°C for 15 minutes, and then washed with DMEM/10% FBS twice to deactivate the enzyme. After washing with DMEM/F12 twice, the tissue was dissociated into single cells through gentle pipetting. All cells dissected from the whole mouse hippocampus were seeded on one well of 6-well plates pre-coated with 20 ng/mL poly-D-Lysine (pdL) and cultured in the DMEM/F12 medium containing 2% B27 supplement, 1% N2 supplement, bFGF (20 ng/mL), EGF (20 ng/mL), 1% Glutamax and 1% P/S, with the medium routinely changed every two days. Accutase (ThermoFisher) was used to digest the NSC culture for passaging. Cortical NSCs were cultured similarly, except that the cells were dissected from mouse cortex at E17.5. Hippocampal Nestin-WT and Nestin-cKO NSCs were transfected with pCAGIG-GFP/HA-YTHDF2 plasmids using Lipofectamine Stem transfection reagent following the manufacturer's instructions (Fisher, STEM00001). For TGFβ signaling inhibition or activation experiments, hippocampal Nestin-WT and Nestin-cKO NSCs were treated with 5 μM SB-431542 and 100 ng/mL TGFβ2, respectively.[85] For YTHDF2 inhibition experiments, hippocampal CD1 NSCs were treated with 25 μM Ebselen (Sigma, E3520)[41]

Tissue processing, immunostaining, EdU staining, and confocal imaging

Tissue processing and immunostaining were performed as described previously.[17] The hippocampal NSCs cultured *in vitro* were fixed with 4% paraformaldehyde (PFA) at room temperature for at least 30 minutes, and then immersed in PBS at 4°C. For tissue histology, mice were perfused with ice-cold PBS for 10 minutes, followed by ice-cold 4% paraformaldehyde (PFA) for 5 minutes. Mouse brains were dissected out and fixed in 4% PFA at 4°C overnight and then immersed in 30% sucrose dissolved in PBS at 4°C for 48 hours. Coronal brain serial sections were cut at 40-μm thickness using a sliding frozen microtome (Leica), sequentially collected in 48-well plates containing anti-freeze solution (500 mL 0.1M PB, 300 mL ethylene glycol, 300 g sucrose), and stored at -20°C. For quantification analysis, every sixth section was used for immunostaining to reconstitute the whole hippocampus.

Before immunostaining, when antigen retrieval was necessary for some antibodies, antigen retrieval of brain sections was first performed by incubating the sections in 1x Target Retrieval Solution (Agilent Dako, S1699) at 95°C for 10 minutes, with gradual cooling down to room temperature (RT). For immunostaining, brain sections were first immersed in the blocking buffer (5% BSA, 10% FBS, 0.3% Triton X-100, 0.01% NaN_3 dissolved in PBS) at RT for 1 hour, and then in the primary antibody solution prepared with the same blocking buffer at 4°C overnight. After washing with PBS for 3 X 10 minutes, brain sections were incubated in the DyLight-405, Alexa Fluor 488, Cy3 or Cy5-conjugated secondary antibodies (Jackson ImmunoResearch, 1:500) and DAPI (Roche, 1:500) prepared in the blocking buffer at RT for 1-2 hours. After a second round of washing with PBS, brain sections were finally mounted on slides with Aqua-Mount Mounting Medium (EMSCO/FISHER, NC9428056).

The confocal images throughout this study were acquired with Zeiss LSM810 confocal microscopy with 20X, 40X, or 63X objectives, and analyzed using software including Photoshop, ImageJ, and Imaris 7.6 software (Bitplane).

For the EdU retaining assay, when analyzed at P14, the subpopulation of NSCs with EdU labeling at P3 that later transitioned to the quiescent state would remain EdU$^+$, whereas proliferating NSCs would have EdU diluted over several cell cycles and become

EdU$^-$ by immunostaining.[17] EdU staining was performed following the manufacturer's instructions (Click-iT EdU Alexa Fluor 647 Imaging Kit, EMSCO/FISHER, C10640) after secondary antibody staining. The antibodies used in this study are listed in the key resources table.

Western blotting analysis

Western blotting experiments were performed following the protocols as described previously.[86] Protein lysates of cultured cells and mouse hippocampal tissues were prepared in the cell lysis buffer containing RIPA lysis buffer (Thermofisher), Phosphatase Inhibitor Mixture, and Protease Inhibitor Mixture. The protein concentration was first determined by Pierce™ Rapid Gold BCA Protein Assay Kit, and then protein lysates were denatured in 1X Sample buffer (NEB) by incubating at 95°C for 10 minutes. About 25 μg of protein from the cell or tissue lysates was loaded on a 4-20% Mini-Gel (BIO-RAD), separated through SDS/PAGE, and transferred into the Trans-Blot Turbo 0.2 μm PVDF membrane (BIO-RAD). After immersing PVDF membranes in 5% milk dissolved in TBS (20 mM Tris/HCl pH 8.0, 50 mM NaCl) at room temperature for 1-2 h, the membranes were incubated in primary antibodies diluted in the blocking buffer (TBS, 0.1% Tween-20, 5% BSA, 0.01% NaN_3) at 4°C overnight. Subsequently, the membranes were incubated in the secondary antibodies conjugated with horseradish peroxidase (HRP) diluted in the blocking buffer at room temperature for 1-2 h. 3X washes with the wash buffer (TBS buffer supplemented with 0.1% TWEEN 20) was conducted after the incubation of primary and secondary antibodies. Finally, Pierce™ ECL Western Blotting Substrate (EMSCO/FISHER) was used to visualize the protein bands on membranes. The antibodies used for western blotting are listed in the key resources table.

RNA extraction and real-time qPCR

RNA extraction and real-time qPCR were performed as described previously.[86] Briefly, the brain tissue or cell culture were homogenized and dissolved in 1 mL TRIZOL (Invitrogen) for 15 minutes on ice, and subsequently, 200 μL chloroform was added. After centrifugation at 12000 g for 15 mins at 4°C, about 400 μL supernatant was carefully transferred to a new tube and mixed with the same volume of ethanol. Then, the mixture was transferred to Zymo-Spin™ IC Column in a Collection Tube from the kit of Zymo RNA Clean & Concentrator™-5. After centrifugation, 400 μL RNA Prep Buffer, 700 μL RNA Wash Buffer, and 400 μL RNA Wash Buffer was sequentially added to the column with each procedure followed by centrifugation. About 15 μL RNase/DNase-free water was used to elute the column to collect the RNA sample. For reverse transcription, about 0.5-1 μg RNA was used to synthesize the cDNA with poly-dT primers according to the manufacturer's instructions of SuperScript III First-Strand Synthesis System (Invitrogen).

qPCR reactions were performed by mixing 10 μL of Fast SYBR Green qPCR Master Mix (ThermoFisher), 1 μL of forward primer (10 μM), 1 μL of reverse primer (10 μM), 6 μL of H_2O, and 2 μL of 1:5 diluted cDNA, and then the StepOnePlus Real-Time PCR System (Applied Biosystems) was used with thermocycling conditions as follows: 95°C for 20 s, 44 cycles of 95°C for 3 s and 60°C for 30 s. The difference value between the Ct values (ΔCt) of the genes of interest and internal control genes within a sample was first calculated, and $2^{(-\Delta\Delta Ct)}$ was used to calculate the fold-change in expression of the genes between two samples. For m^{6}A-IP-qPCR and YTHDF2-RIP-qPCR, the level of mRNAs pulled down by anti-m^{6}A and anti-YTHDF2 antibodies was normalized to that of the GFP mRNA spike-in, which was synthesized by *in vitro* transcription using mMessage mMachine T7 Ultra kit (ThermoFisher, AM1345) and did not contain any modifications. The qPCR primers used in this study are listed in Table S1.

RNA decay assay, RNA-seq, m^{6}A-seq, YTHDF2-RIP-seq, and data analyses

RNA decay assay was performed by treating the hippocampal NSC culture with transcription inhibitor Actinomycin D (Sigma, 5 μM). Then, the RNA from the cells collected at three time points after addition of Actinomycin D (0, 2 h, 4 h) was extracted with TRIZOL, and used for RNA-seq and qPCR measurement.

RNA-seq libraries of cultured WT and cKO NSCs at 0, 2 h, 4 h post Actinomycin D treatment were prepared based on the SMART-seq2 method as previously described.[86] For reverse transcription, 3.2 μL RNA (100 ng/μL), 0.25 μL RNase inhibitor (NEB) and 1 μL CDS primer (10 μM, 5′-AAGCAGTGGTATCAACGCAGAGTACT30VN-3′) were mixed and incubated at 70°C for 2 minutes, with cooling down on ice. Then, 0.5 μL of DTT (100 mM), 0.3 μL of $MgCl_2$ (200 mM), 1 μL of dNTPs (10 mM), 0.25 μL of RNase inhibitor (NEB), 1 μL of TSO primer (10 μM, 5′-AAGCAGTGGTATCAACGCAGAGTACATrGrGrG-3′), 2 μL of 5X SMARTScribe RT buffer (Takara), and 0.5 μL SMARTScribe reverse transcriptase (Takara) was added. The thermocycling conditions of the reverse transcription reaction were as follows: 42°C for 90 minutes, 10 cycles of 50°C for 2 minutes and 42°C for 2 minutes, and then 70°C for 15 minutes. To amplify the full-length cDNA, 17.25 μL nuclease-free water, 2 μL of the reverse transcription reaction, 2.5 μL of 10X Advantage 2 buffer (Takara), 2.5 μL of dNTPs (2.5 mM), 0.25 μL of IS PCR primer (10 μM, 5′-AAGCAGTGGTATCAACGCAGAGT-3′) and 0.5 μL Advantage DNA Polymerase (Takara) were mixed, and thermocycling conditions of PCR were as follows: 94°C for 3 minutes, 8 cycles of 94°C for 15 s, 65°C for 30 s and 68°C for 6 minutes, followed by 72°C for 10 minutes. PCR products were purified with 0.8X AMPure XP beads (Beckman Coulter), eluted in nuclease-free water, and quantified according to the instructions of Qubit dsDNA HS assay kit (ThermoFisher). Tagmentation of cDNA was performed by first mixing 2 μL cDNA (50 pg/μL), 2.5 μL 2X TD buffer (20 mM Tris/pH 8.0, 10 mM $MgCl_2$, and 16% PEG 8000) and 0.5 μL adaptor-loaded Tn5 transposase (Lucigen), which was then incubated at 55°C for 12 minutes. The reaction was then terminated by adding 1.25 μL of 0.2% SDS (Fisher) and incubated at RT for 10 mins. The subsequent PCR reaction was performed by adding 16.75 μL H_2O, 1 μL of Nextera i5 primer (10 μM), 1 μL of Nextera i7 primer (10 μM), and 25 μL KAPA HiFi hotstart readymix (EMSCO/FISHER), with the thermocycling conditions as follows: 72°C for 5 minutes, 95°C for 1 minute, 14 cycles of 95°C for 30 s, 55°C for 30 s and 72°C for 30 s, then 72°C for 1 minute, and 4°C indefinitely. PCR products were then purified twice with 0.8X AMPure XP beads, eluted in nuclease-free water, and quantified with Qubit dsDNA HS assay

kit. Different libraries from 3 WT and 3 cKO cultured NSCs at different time points post Actinomycin D treatment were quantified using KAPA library Quantification kit and pooled together at equal molar amounts. The average fragment size of the final library fragment was determined as 420 bp by using a bioanalyzer (Agilent), and the concentration of the final library was determined by qPCR with KAPA Library Quantification Kit. The final library was subjected to a NovaSeq 6000 System (Illumina) and 1x100 bp single-end sequencing was performed.

Raw sequencing data from RNA-seq were initially demultiplexed with bcl2fastq2 v2.17.1.14 (Illumina). Adaptors were subsequently trimmed using Trimmomatic v0.32 software, with the MINLEN setting at 18.[80] The STAR v2.5.2a was used to perform alignment of reads to GENCODE mouse reference genome GRCm38.p6.[79] The multimapping and chimeric alignments were discarded, and only uniquely mapped reads were quantified at the gene level and summarized to gene counts using STAR-quantMode (GeneCounts). Further analyses were performed in R (v3.6.0). Differential gene expression analysis between WT and cKO NSCs was performed using DESeq2 v1.36.0, with genes whose average counts were lower than the 10 discarded,[77] and identified significantly upregulated (Padj < 0.1; fold-change > 1.5) and downregulated (Padj < 0.1; fold-change < 2/3) genes between WT and cKO NPCs were used for Gene Ontology (GO) and pathway enrichment analysis using Metascape Database[78] (Table S2). As shown in Figure S2I, the fold-change of Gene i between cKO and WT samples at 2 h ($FC(2h)_i$) and 4 h ($FC(4h)_i$) after Actinomycin D treatment was first normalized with $FC(0h)_i$, and then the normalized fold-change ($NorFC_i$) at 2 and 4 hpa would be used to indicate the decay speed.[25] The higher the $NorFC_i$, the slower the RNA decay of Gene I would be. A gene whose $NorFC(2h)_i$ or $NorFC(4h)_i$ was bigger than 1.2 was defined as a gene that undergoes slower decay in cKO NSCs. TPM (transcripts per million) values of selected genes of were converted to row Z-scores per gene for visualization in heatmaps.

m^6A-seq was performed and analyzed as previously described with minor adjustments.[87] After washing the Protein A beads twice with m^6A-IP-buffer (50 mM Tris/HCl pH 7.4, 150 mM NaCl, 0.1% IGEPAL CA-630), 3 μg of m^6A antibody (EMSCO/Fisher, ABE572) or 3 μg rabbit IgG was first incubated with Protein A beads at 4°C for 1 hours, followed by two washes with m^6A IP-buffer again. Then the Protein A beads were reconstituted with 0.5 ml of m^6A-IP-buffer containing 3 μL RNAase inhibitors (NEB, 40 U/μL), mixed with 2.5 μg of RNA extracted from 3 Nestin-WT cultured NSC samples (with 200 ng RNA saved as input), and incubated at 4°C for 2 hours. After washing with m^6A-IP-buffer twice and then high-salt wash buffer (50 mM Tris/HCl pH 7.4, 500 mM NaCl, 0.1% IGEPAL CA-630) twice, the m^6A-tagged RNA bound to the beads was eluted with m^6A-IP-buffer containing 6.7 mM N^6-Methyladenosine compound (Sigma-Aldrich; M2780) by incubating at 4°C for 1 hour. Finally, the RNA in the eluates was purified with the kit of Zymo RNA Clean & Concentrator™-5, with 8 μL water used for elution. The eluted m^6A-tagged RNA was used to prepare the library following the protocol of RNA-Seq library preparation, except the reverse transcription step. Because of the low amount of RNA, the reverse transcription was performed based on the SMART-Seq3 method.[88] 1 μL eluted RNA or 1 μL input RNA (20 ng/μL), 0.1 μL RNase inhibitor, 0.625 μL 40% PEG 8000, 0.25 μL dNTP (10 mM), 0.25 μL CDS primer (10 μM) and 0.8 μL H_2O were mixed and incubated at 70°C for 2 minutes. Then, 0.1 μL Tris/HCl (1M, pH 8.3), 0.16 μL NaCl (1M), 0.125 μL of $MgCl_2$ (100 mM), 0.05 μL GTP (Thermo, R1461,100 mM), 0.4 μL of DTT (100 mM), 0.0625 μL of RNase inhibitor, 1 μL of TSO primer (10 μM), and 0.2 μL Maxima H RT enzyme (Fisher, EP0753, 200U/μL) was added. The reverse transcription reaction was performed at 42°C for 90 minutes, followed by 10 cycles of 50°C for 2 minutes and 42°C for 2 minutes, and then 70°C for 15 minutes. Then the cDNA was amplified with KAPA HotStart PCR Kit (Roche, KK2502), quantified with Qubit kit and tagmented with adaptor-loaded Tn5 transposase. The input and m^6A-IP libraries of cultured NSCs of 3 biological replicates were pooled together and loaded on the Novaseq X+ system for 1x100 bp single-end sequencing. The demultiplexing, adaptor-trimming, read alignments of m^6A-seq library was performed following the same protocol of RNA-seq. TPM (transcripts per million) values of all genes were calculated, and genes whose average TPM were lower than the 0.1 were discarded. m^6A-tagged genes were identified following the protocol described previously.[87] For each gene, its TPM ratio of m^6A-IP/Input was first calculated, and then its Z score was then calculated by the ratio (m^6A-IP/Input) divided by the mean of the group to reflect the relative m^6A level of each gene on a transcriptome-wide scale.[89] Genes whose Z scores were higher than 0 were identified as genes with modest to high m^6A levels.

For YTHDF2-RIP-seq, the lysates of cultured Nestin-WT NSCs with ~90% confluence on a 10 cm-dish were prepared in 1 mL RIP-buffer [50 mM Tris/HCl (pH 7.4), 150 mM NaCl, 0.5% IGEPAL CA-630, 2 mM EDTA (pH 8.0), 0.5mM DTT, 0.3 U/μL RNAase inhibitor, Phosphatase Inhibitor Mixture, and Protease Inhibitor Mixture]. Meanwhile, 3 μg of YTHDF2 primary antibody (Aviva systems) or 3 μg rabbit IgG was first incubated with Protein A agarose beads (30 μL) at 4°C for 2 h. After two washes with RIP buffer, the Protein A beads were mixed with 0.5 mL lysates of NSCs and incubated at 4 °C for overnight. Then the beads were washed with cell lysis buffer three times, and 1mL TRIZOL was added into the beads to extract the RNA, which was pulled down by YTHDF2 antibodies. The library preparation of the IgG and YTHDF2-pulldown RNA from 3 biological replicates, sequencing of the library, and data analysis were performed following the same protocol as m^6A-Seq. To identify YTHDF2-bound genes, the TPM ratio of YTHDF2-IP/IgG for each gene was calculated, and the Z score of each gene was then obtained by the ratio (YTHDF2-IP/IgG) divided by the mean of the group to reflect the relative YTHDF2-binding level of each gene. We set Z score > 0 as a threshold to identify genes with relatively modest to high YTHDF2-binding levels.

QUANTIFICATION AND STATISTICAL ANALYSIS

The number of cells positive for single or multiple markers within brain sections or cultured cells *in vitro* were counted with the "Spots" function of Imaris software. We infer neural stem cell quiescence by analysis of the expression of proliferation markers *in vitro* and *in vivo*. For staining intensity analysis, cell-attached coverslips were put in the same well and processed in parallel with the same

primary/secondary antibodies, and the corresponding images were taken and processed using the same settings. The sum of intensity of each channel was measured using the "Measure" function of ImageJ software and used for quantification. All Nestin$^+$YFP$^+$ cells in the DG were scored as NSCs at P7; for the brain sections dissected from mice older than P14, only the Nestin$^+$YFP$^+$ or Nestin$^+$Hopx$^+$ cells with radial glia-like morphology which were localized in the subgranular zone (SGZ) of DG were scored as NSCs. The area of SGZ in brain sections was calculated by multiplying the length of SGZ measured with ImageJ software by the z-axis thickness. For quantification analysis in the in vivo study, the average value from 3 or 4 different sections was used for the quantification of one animal. For *in vitro* studies, at least five regions of the cell culture derived from one mouse were randomly selected for imaging, and the average value was used for quantification analysis as one biological replicate. The exact number of mice analyzed throughout this study was listed in figure legends. An estimate of variation within each group of data was calculated with standard error of the mean (SEM) for all statistical analyses. Unpaired two-tailed or one-tailed Student's *t*-test, Welch's t-test or one-way ANOVA analysis was conducted using Excel, R, or GraphPad Prism software to calculate the significant differences, which were indicated as ns (not significant), *$P < 0.05$, **$P < 0.01$, and ***$P < 0.001$.